Glacier Surge Dynamics at the West Kunlun Shan inferred from Satellite Remote Sensing

（衛星遠地観測に基づく西クンルン山脈における氷河サージならび流動構造）

Takatoshi Yasuda

Department of Natural History Sciences, Graduate School of Science,

Hokkaido University

Submitted for the degree of Doctor of Philosophy

March 2015

Contents

Abstract

Surge-type glaciers oscillate between short period of fast flow and long period of slow flow, called active phase and quiescent phase, respectively. In active phase, large ice masses transport from upper glacier to down-glacier that cause advance in it terminus position and thinning and thickening occurs on lower and upper glacier. Glacier surging happen without external factor like climate changes and this unusual surge behavior obscure climate signal on glaciers. The response to climate changes generally assume that reduction in glacier area and ice thickness result from surface mass balance in steady-state. Surge-type glaciers are not suitable as index of climate changes and their distribution have great impotence. Surge-type glaciers distribute around world and only about 1% of glaciers are consider as surge-type but some surge-type glaciers still are missed and adds small numbers to the surge inventory yearly basis. Furthermore, exact surge mechanisms are still elusive and temporal velocity over surging phase are valuable to clarify dynamics of glacier surging.

In this thesis, I study dynamics of mountain glaciers in West Kunlun Shan, located in northwestern Tibetan plateau using satellite remote sensing techniques. The thesis includes the following two topics:

(1) Surge-type glaciers in West Kunlun Shan

Surge-type glaciers in WKS had been missed due to remote location and logistical problems and cause large uncertainty to estimate climate changes through reduction in glacier area and ice thickness. I first identified surge-type glaciers in WKS based on temporal velocity maps derived from satellite SAR datasets from 1992, changes in glacier terminus position from Landsat optical imageries from 1972, and visible surface features indicative of surging signal. Results revealed distribution of surge-type glacier and general characteristics of surge-type glacier in WKS. Of thirty one major glaciers, 11 glacier were confirmed as surge-type glaciers and 6 glaciers were suspected. Flow speed gradually increased up to ~200-1000 m/year in decade-long active phase and decelerated ~0-30m/year in quiescent phase. Since no glacier repeated glacier surging during observation period, surge cycle estimated at least 42 years. These decades-long duration in active and in quiescent phase, which was similar to the Svalbard-type surges.

(2) Glacier surge dynamics at the West Kunlun Shan

Triggering mechanisms of glacier surge are still elusive. From cumulative studies, two possible mechanism are proposed to explain different velocity development in active phase.

One is the hydrological regulation mechanism based on the observations of glacier surging at the Variegated Glacier, Alaska. The glacier flow abruptly switches between quiescent velocity and surging velocity, initiating in winter and terminating in

summer. The duration of surging is typically 1-3 years and quiescent phase is in the order of decades. It seems that the development of surging is coincided with changes in hydraulic systems.

On the other hand, the thermal regulated mechanism is proposed based on the observations of surge-type glaciers at Svalbard. Glaciers at Svalbard are poly-thermal glaciers, overlying sedimentary beds. The peak flow speed is generally slower compared to the Alaskan surges. The Svalbard-type surges generally have years-long surging phase and long quiescent phase which continues decades to over a century. The development of surging gradually initiates and terminates in any season. It presumes that pressure melting produced amounts of meltwater at the bottom, leading to the initiation of glacier surging.

Three glacier had been surging since early 2000s in WKS. Here I focused on two surging glaciers in WKS and their flow dynamics using different satellite SAR datasets from 2003 to 2014, up to 46 days and 11 days temporal resolution with ALOS/PALSAR imageries from 2007 to 2011 and TerraSAR-X imageries from 2012, respectively. Results reveals that surging flow accelerated and decelerated over seven years accompanied with seasonal fluctuation. The surging flow speeded up during fall to winter and slowed down in summer. The amplitude of peak velocity reached up to 180-200% in 2013. This indicated that surface meltwater could be delivered into the bottom during surging, influencing the basal slip though the englacial water storages and discharge processing.

Acknowledgment

I would like to express my sincere gratitude to everyone who has helped and has encouraged me throughout my graduate course. First of all, I owe my cordial gratitude to my supervisor, Professor Masato Furuya for his guidance, close support, valuable comments and discussions during the course of my graduate student at Hokkaido University.

I would like to thanks Professor Kousuke Heki, Professor Junji Koyama, Professor Kiyoshi Yomogida, Professor Kazunori Yoshizawa, Professor Makoto Murakami, Associate Professor Kazuhisa Chikita, Associate Professor Shin Sugiyama, Dr. Akiko Takeo and the members of the solid seminar for their constructive comments. University. In particular, Professor Shin Sugiyama gave me considerable comments and valuable discussions from the standpoint of a glaciologist. I want to thank Dr. Akiko Takeo. I received considerable encouragement from her. Special thanks also to all my colleagues in the Space Geodesy laboratory in Hokkaido

ERS1/2 and ENVISAT data are copyrighted by European Space Agency and were provided under Cat-1 project 7344. PALSAR level 1.0 data in this study were provided by the PALSAR Interferometry Consortium to Study our Evolving Land Sur-

face (PIXEL) and the ALOS 3rd PI project under cooperative research contracts with the Japan Aerospace Exploration Agency (JAXA). The ownership of PALSAR data belongs to JAXA and the Ministry of Economy, Trade and Industry. TerraSAR-X (TSX) data are copyrighted by the German Aerospace centre (DLR) and were provided under TSX proposal LAN1257. I would like to thank JSPS DC-2 fellowship for a grant that makes it possible to complete this study.

Chapter 1

Introduction

1.1 Surge-type glaciers

Surge-type glaciers oscillate between short period of fast flow and long period of slow flow, called active phase and quiescent phase, respectively. In active phase, large ice masses transport from upper glacier to down-glacier that cause advance in it terminus position and thinning and thickening occurs on lower and upper glacier. Glacier surging happen without external factor like climate changes and this unusual surge behavior obscure climate signal on glaciers that assume reduction in glacier area and ice thickness result from surface mass balance in steady-state, hence surge-type glaciers are not suitable as index of climate changes and their distribution have

great impotence. Surge-type glaciers distribute around world and only about 1% of glaciers are consider as surge-type [Jiskoot et al., 2000] but some surge-type glaciers still are missed. The number of surge-type glaciers in actually increasing year by year [Rankl et al., 2014].

1.2 High Mountain Asia and West Kunlun Shan

High Mountain Asia (HMA), including Himalaya, Hindu Kush, Karakoram, Pamir, Tien Shan, and West Kunlun Shan, is the largest glaciated areas outside the two ice sheets, and a mass loss of about 30 Gt/yr was estimated for the period between 2003 and 2009 [Gardner et al., 2013]. The meltwater from the glaciers at HMA are also important resources in the nearby billions of people. However, because of the sparse spatial and temporal coverage of satellite remote sensing data and the paucity of ground-based glaciological observations due to the remoteness and logistic problems, the details of the glacier changes at HMA over the past decades still contain large uncertainties [Bolch et al., 2012, Gardner et al., 2013].

Surge-type glaciers are clustered in some regions around HMA, including Pamir [Dolgoushin and Osipova, 1975], Tien Shan [Liu et al., 1998; Glairin, 2010; Xie and Liu, 2010], south east and northern Tibetan Plateau [Zhang, 1992, Guo et al., 2013], Karakoram [Hewitt, 2007, Quincey et al., 2011] and West Kunlun Shan [Yasuda and Furuya, 2013]. Comprehensive glacier inventory of surge-type, however, is developed only on Karakoram [Rankl et al., 2014] and in the other subregions it is very

likely that surge-type glaciers are unidentified.

Surge-type glaciers in WKS had been overlooked due to remote location and logistical problems and cause large uncertainties to evaluate the effect of climate changes on the reductions in glacier areas and ice thickness. We first identified four surging glaciers in WKS based on temporal velocity maps derived from satellite SAR datasets [Yasuda and Furuya, 2013]. Distribution and characteristics of surge-type glaciers, however, were remain uncertain.

1.3 Outline of this study

I work on glacier flow dynamics in West Kunlun Shan (WKS), located in north-western Tibetan plateau, China, using satellite remote sensing techniques. The main objectives of this study are: 1) to reveal distribution and general characteristics of the surge-type glaciers in the WKS; to clarify glacier surge dynamics in the WKS. Each of the studies is described in detail in Chapter 3 and Chapter 4, respectively. The contents of this thesis are summarized as follows;

Chapter 2: gives a brief overview of Satellite based Synthetic Aperture Radar and ice flow dynamics.

Chapter 3: In this chapter, I will describe in detail the methodology and datasets to identify surge-type glaciers based on remote sensing techniques, and distribution and general characteristics of surge-type glaciers in WKS. I will contribute on estimation of the effect of climate changes on the reductions of glacier area and ice

thickness.

Chapter 4: I will describe glacier surge dynamics at the WKS and possible mechanisms based on the spatial-temporal velocity changes over a decade-long surging flow. I analysed ALOS/PALSAR and TerraSAR-X imageries whose temporal resolution are 46 days and 11 days, respectively. No previous studies have examined the velocity evolution of surging glaciers with such a high temporal resolution.

Chapter 5: I will conclude this study.

Chapter 2

SAR and glacier flow map

2.1 Synthetic Aperture Radar and ice flow dynamics

SAR (Synthetic Aperture Radar), one of the remote sensing techniques usually on-board a satellite platform, is a side-looking active radar system, which enables us to detect Earth surface properties regardless of weather condition and day/night time. One notable feature in SAR system is the spatial resolution, which depends on only the antenna size and the bandwidth of a transmitted pulse. For a real aperture radar system, spatial resolutions in the radar line-of-sight (range) direction ΔR and the platform (azimuth) direction ΔA depend on pulse width and beam width expressed as

$$\begin{aligned} \Delta R &= \frac{c\tau_0}{2}, \\ \Delta A &= \frac{\lambda R_c}{D_A}, \end{aligned} \tag{2.1}$$

where c is the speed of light, τ_0 is the pulse width, λ is the wavelength, R_c is the slant range between the antenna and the target and D_A is the antenna size along the azimuth direction. For SAR, high spatial resolution in range ΔR and azimuth ΔA is archived by pulse compression and creating a large antenna synthetically along the platform path, theoretically expressed as

$$\begin{aligned} \Delta R &= \frac{c}{2B_R}, \\ \Delta A &= \frac{D_A}{2}, \end{aligned} \tag{2.2}$$

where B_R is the bandwidth and D_A is the antenna. In the case of ALOS/PALSAR (D_A = 8.90m, B_R = 28 MHz in the fine beam single polarimetry mode), range × azimuth resolution ideally reaches up to 5.4 × 4.5 m. Unlike other geodetic methods such as GNSS, SAR system cannot observe continuously over time. That is temporal resolution depends on the revisit time of the platform, and also SAR cannot observe deeply incised area where transmitted pulse is overlapped or shadowed due to geometric effects resulting from the side-looking radar system.

SAR-based techniques for measuring glacier flow dynamics have developed rapidly

since 1993 [Joughin et al., 2010]. Goldstein et al. [1993] first applied SAR interferometry (InSAR) to observe the Antarctic ice stream and soon after many researchers used InSAR method to detect ice sheet motion in Greenland [Joughin et al., 1995, Rignot et al., 1995, Joughin et al., 1996, Rignot, 1997]. Offset tracking methods are less accurate and lower in terms of the spatial resolution than InSAR method, but enable us to detect large displacements along both slant-range and azimuth direction can be detected from single SAR image pair, as long as phase coherence or surface features are preserved. Gray et al. [1998] first applied speckle (coherent) tracking to estimate the glacier motion in Antarctica and later Strozzi et al. [2002] introduced intensity tracking to detect rapid ice flow caused by glacier surging at Monacobreen in Svalbard. To obtain full three-dimensional flow components using SAR-based method, independent three line-of-sight observations in the same period are necessary. However, this situation is rarely archived for satellite SAR. Instead, researchers used a parallel flow assumption in which the direction of glacier flow is provided from the surface slope [Rignot et al., 1996, Joughin et al., 1996, Rott et al., 1998, Mohr et al., 1998, Joughin et al., 1998] or a flow line parallel to the glacier margins [Mattar et al., 1998, Sund et al., 2014].

Chapter 3

Surge-type glaciers in West Kunlun Shan

3.1 Introduction

Due to the global warming trend over the last and present centuries, meltwater from snow cover and glaciers outside the Antarctic and Greenland ice sheets is estimated to significantly contribute to the global sea level rise despite their smaller size of the areas [Meier et al., 2007, Gardner et al., 2013]. High Mountain Asia (HMA), including Himalaya, Hindu Kush, Karakoram, Pamir, Tien Shan, and West Kunlun Shan, is the largest glaciated areas outside the two ice sheets, and a mass loss of about 30 Gt/yr was estimated for the period between 2003 and 2009 [Gardner et al., 2013]. The meltwater from the glaciers at HMA are also important resources in the nearby billions of people. However, because of the sparse spatial and temporal coverage of satellite remote sensing data and the paucity of ground-based glaciological observa-

tions due to the remoteness and logistic problems, the details of the glacier changes at HMA over the past decades still contain large uncertainties [Bolch et al., 2012, Gardner et al., 2013].

The West Kunlun Shan (WKS) area is one of the highest elevation regions on the Earth (Fig. 3.1), and due to the remoteness and harsh environment, there have been few ground-based glaciological studies [Zhang and Jiao, 1987, Zhang et al., 1989, Thompson et al., 1995]. As such, satellite remote sensing image analyses have been used to evaluate the temporal changes in the WKS area. Based on Landsat imageries from 1970 to 2001, Shangguan et al. [2007] reported a slight retreat with large uncertainties (0.4%) of the total area. Whereas the glaciers at HMA are overall presumably losing mass, the WKS glaciers are estimated to have gained mass with equivalent elevation changes of 0.17±0.15 m/yr from 2003 to 2009 [Gardner et al., 2013], based on the differences between ICESat/GLAS laser altimetry data and the digital elevation maps from Shuttle Radar Topography Mission; similar mass gain trend is also reported at the Karakoram region [Gardner et al., 2013]. Glacier dynamics at the WKS are even more uncertain. However, based on radar image analyses, Yasuda and Furuya [2013] examined the spatial-temporal changes in the surface velocities of 36 glaciers in the WKS, and first identified four glaciers as surge-type at WKS.

Surge-type glaciers exhibit cyclic behavior between an active phase and a quiescent phase with a recurrent interval of decades to centuries [Meier and Post, 1969, Raymond, 1987, Harrison and Post, 2003]. In a shorter (<~5 years) active phase, the glacier flow velocity increases by several times or orders-of-magnitude compared

to the quiescent phase. Because the significant volume of the entire ice masses are transported to down glacier, glacier surge leads to dramatic changes in their surface height and terminus positions, forming newer crevasses and tear-shaped moraine. In a longer (a decade- to century-long) quiescent phase, surge-type glaciers flow slowly or become stagnant. Imbalance flow causes the retreating and thinning in the lower part, and ice mass is accumulated for the next surge.

To identify surge-type glaciers is important to adequately interpret the glacier mass balances at any glaciated regions [Yde and Paasche, 2010]. Glacier mass balances are usually estimated on the assumption of non-surge type glaciers whose dynamics are only affected by long-term climate changes. For instance, a significant increase of ablation at non-surge type glaciers will lead the recession of frontal positions. At surge-type glacier, however, the retreat of frontal position is simply a snapshot of the normal surge cycle. Nonetheless, in contrast to other glaciated regions in the world, the distribution of surge-type glaciers at WKS was unknown. Moreover, although an increasing number of surging episodes in the Karakoram has been suggested [Quincey et al., 2011, Copland et al., 2011], the effect of global warming on the dynamics of surge-type glaciers remains uncertain and deserves further investigations.

3.2 Study area

West Kunlun Shan (WKS), located in the northwestern Tibetan plateau (Fig. 3.1), is the one of the highest region where most of the peaks are 6500 m a.s.l. and the highest is Luishi Shan at 7167 m. There are 278 glaciers almost debris free (<3%) with total area 2711.57 km^2 along the main ridge [Shangguan et al., 2007, Scherler et al., 2011] which divides the mountain into south and north; on the southern slope where elevation gradually reduces toward the typical shape of a plateau surface and no glaciers develop below 5200m [Zhang and Jiao, 1987]; on the northern slope where relatively long-steep glaciers flow into deep incised valley, and some glaciers develop below 5000m [Zhang et al., 1989]. Of the numerous mountain glaciers in the High Mountain Asia (HMA), WKS belongs to the extreme continental setting, because it is one of the driest and coldest region around Tibetan plateau; the annual average precipitation and temperature estimated near the equilibrium line altitude (5930m) is 300 mm and -13.9 deg. C, respectively [Zhang et al., 1989]. Accumulation and ablation mainly occur during May-August [Zhang et al., 1989], influenced partly by East Asian Monsoon after the westerly jet shift to the north in April. Also moisture recycling in Tibetan plateau could play a negligible role [Maussion et al., 2014].

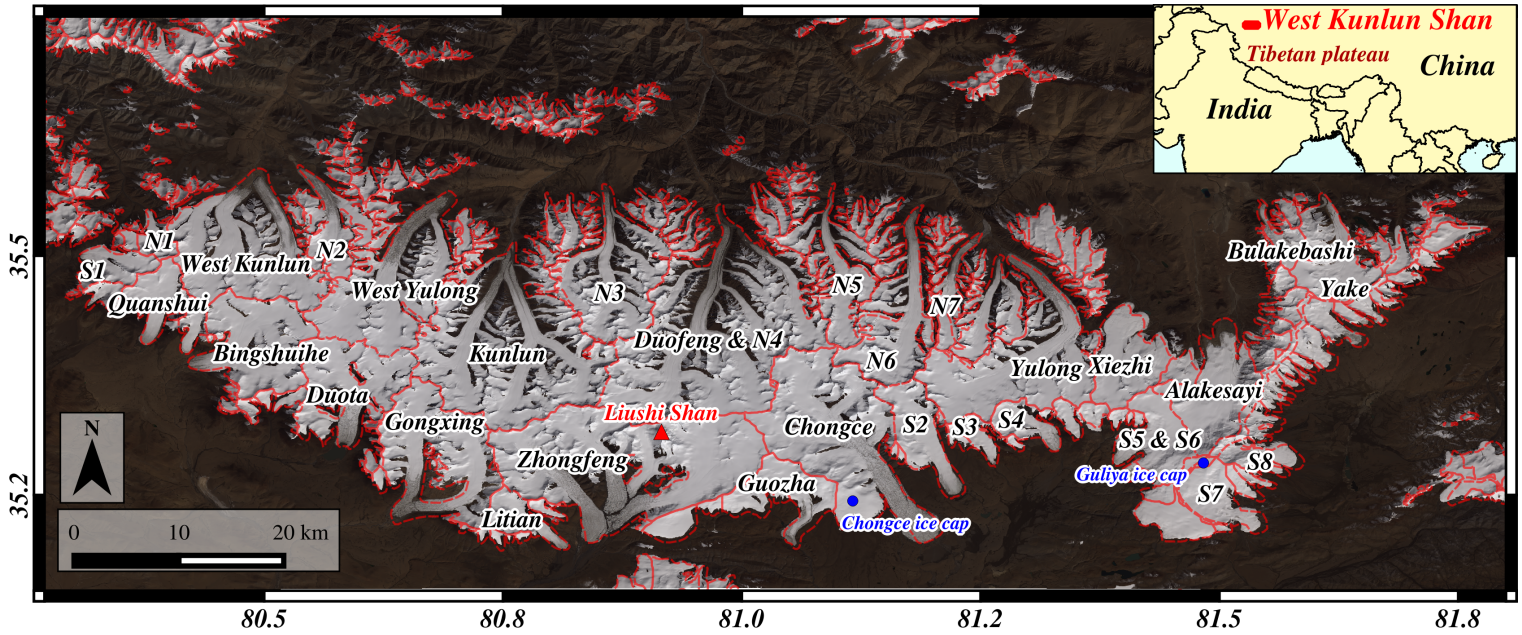

Figure 3.1: West Kunlun Shan on Landsat 8 true color image from Sept. 27, 2013. Red dashed lines show glacier outlines from Randolph glacier glacier inventory version 3.0 [Pfeffer et al., 2014]. Glacier names are from NSIDC world glacier inventory [Ma et al., 1989, Zheng et al., 1989]. Those glaciers with “N” or “S” indicate no named glaciers in the northern and southern slope, respectively.

3.3 How to identify surge-type glaciers?

Criteria to distinguish surge-type glaciers from normal (non-surge-type) glaciers by remote sensing are mainly the visible surface features including a surge advance, elongated moraine loops, a surge front propagation marked surge bulge and a completely crevassed glacier [Jiskoot, 2011]. Ice mass flow of surge-type glaciers differs from the balance velocity of normal glaciers. The flow speed in the quiescent phase is stagnant or much lower than the balance flow but is 10-1000 times faster in active phase. This quiescent (surging) velocity is a strong evidence to identify surge-type glaciers, when temporal velocity maps are available. In this section, I will describe the processing method to detect surface velocity and changes in terminus position using satellite SAR from 1992 and Landsat imageries from 1972, and how to identify surge-type with the available surge evidences.

3.3.1 SAR archived data and temporal velocity map

SAR data processing

I used satellite SAR datasets during 1992, 1996 and 2003-2014 acquired with five different sensors whose basic parameters are summarized in table 3.1. Processed SAR image pairs which are not necessarily operated the study area with the nominal repetition interval are listed in table 3.2. Using the software package, Gamma [Wegmüller and Werner, 1997], the image pairs were first co-registrated based on

each orbit data and SRTM4 DEM (Shuttle Radar Topography Mission digital elevation model; http://srtm.csi.cgiar.org) [Jarvis et al., 2008] to reduce the stereoscopic effect. I used the intensity tracking algorithm, which was the only method that can detect fast-flowing glacier velocity between long time separation [Strozzi et al., 2002]. This algorithm was based on maximizing the cross-correlation of the pixel window moving on the slave image. Local image offsets with signal-to-noise ration (SNR) were output as range offset and azimuth offset that were displacements along radar line of sight and platform direction. The parameters for the offset tracking were set as Table 3.1. Range and azimuth steps were chosen so that the pixel size could match ~50m×50m in accordance with the spatial resolutions of each satellite. Window size basically set as 5 times of the steps, except for TSX data which were set as 256×256 pixels to catch fast movement of surging glacier. The offsets and SNR were geocoded onto UTM coordinate with ~50m×50m ground resolution and were normalized to meter per year.

Making a glacier mask

I created a glacier mask based on a semi-automatic algorithm with a Landsat satellite imagery [Hendriks and Helsinki, 2007] to separate between glacier area and non-glacier area. I used a cloud free imagery acquired with LSAT8/OLI in Sept. 2014 to calculate the Normalized Difference Water Index (NDWI) and the Normalized Difference Snow Index (NDSI). To delineate the water area and the snow area, the NDWI and NDSI threshold value as 0.09 and 0.50, respectively. A morphological

opening with 4-connected neighborhood applied to generated mask to sieve small area fewer than 110 pixels. Finally, I manually adjusted the mask to fit glacierized area including changes in front position of surge-type glacier and a glacier snout covered with glacier debris.

Filtering anomalous offsets

Suspicious offsets were semi-automatically removed based on a magnitude of range and azimuth offsets, SNR value, and the glacier area mask. Threshold values for each filtering were manually determined and a size of filter window was set as 3×3 pixels. First of all, the velocities above 1500m/yr were rejected as error offsets. This value was considered from maximum surging speed in WKS. Flow speed in the accumulation area was generally slow, and I rejected offsets over 50 m/yr located above 6200m. The SNR was often used to indicate the reliable offsets. The offsets were rejected with SNR lower than 2, or if SNR was lower than 5 and the velocities exceeded 100m/yr. Rock area and glacier area were separated using the mask. For normal flow, the offsets were rejected if the velocities exceeded 140m/yr. Threshold value for surging ranged from 100m/year to 1500m/year that was depended on progress of surge phase. Small area, that have fewer than 50 pixels with 4-connected neighborhood, were removed with the morphological opening. Finally, median filter was performed to reject discontinuous offsets.

Surface velocity maps based on a parallel flow assumption

There are several approaches to convert the offsets to surface velocity according to available look directions of SAR images. We can detect full 3D flow components converting the offsets observed from the ascending and descending orbit in almost same period without any assumptions [Nagler et al., 2012, Neelmeijer et al., 2014]. This situation is rarely archived for many satellite SAR. When only one path data available, surface velocity is estimated based on a parallel flow assumption.

I converted offsets to surface velocity based on a parallel flow by Joughin et al. [1998] that assumed the glacier flows on the local slope of the glacier surface. The local slope was estimated from the fore-mentioned SRTM-4 data. This assumption, however, does not valid for accumulation (ablation) area where the parallel flow is not valid due to emergence (submergence) flow [Mattar et al., 1998]. Also it lead to over/under-estimations of glacier flows in unsteady state. Critical error results from differences between slope direction and flow direction. Median filter and Gaussian filter applied to components of slope vector to smooth the local slope. I assumed that changes in surface elevation in the active phase were smaller than horizontal displacement and effect on the surging flow speed was less, especially during short time separation with TerraSAR-X data.

Flow profiles along glacier centerline

Setting a centerline with tick interval of 100m at each valley glacier from the head toward the down-glacier, I estimated the surface velocity profiles by averaging the data over a 200×200m^2 area and regarded the standard deviations as the estimated errors. When the number of data samples was less than half of the total pixel numbers at each averaging area, I considered them as missing data.

Satellite/Sensor	ERS1-2/AMI	ENVISAT/ASAR	ALOS/PALSAR	TerraSAR-X
Authorities	ESA	ESA	JAXA	DLR
Band (wavelength)	C (5.66cm)	C (5.62 cm)	L (23.61 cm)	X (3.01 cm)
Data coverage	1992, 1996	2003 - 2007	2007 - 2011	2012 - 2014
Mode	Image/tandem	Image	FBS/FBD	Stripmap
Spatial res. $*$ (m)	7.9×3.9	7.8×4.05	4.68 / 9.36 × 3.14	0.9 × 2.05 m
recurrent period	35/1 days	35 days	46 days	11 days
parameters for offset tracking				
window size pixels $*$	128 × 256	35 × 70	60 × 90	256 × 256
Step pixels $*$	16 × 20	7 × 14	12 × 18	50 × 25
SNR threshold $*$	>2.0	>3.0	>3.0	>2.0

$*$(range × azimuth)

Table 3.1: Satellite SAR sensors and basic properties

Table 3.2: Detailes of the processed SAR image pairs

satellite/sonsor	path	mode	AorD	master	slave	Bperp (m)[a]	span (day)
ERS/SAR	248	image	D	Nov-10-1992	Dec-15-1992	-141.4	35
ERS/SAR	248	tandem	D	Apr-11-1996	Apr-12-1996	-102.4	1
ERS/SAR	248	tandem	D	May-16-1996	May-17-1996	-114.4	1
ERS/SAR	477	tandem	D	Apr-27-1996	Apr-28-1996	-101.9	1
ENVISAT/ASAR	248	image	D	Nov-07-2003	Dec-12-2003	283.7	35
ENVISAT/ASAR	248	image	D	Sep-17-2004	Oct-22-2004	39.3	35
ENVISAT/ASAR	248	image	D	Mar-11-2005	Apr-15-2005	-62.4	35
ENVISAT/ASAR	248	image	D	Jan-20-2006	Mar-31-2006	18.0	70
ENVISAT/ASAR	248	image	D	Mar-16-2007	Apr-20-2007	-386.2	35
ALOS/PALSAR	515	FBS-FBS	A	Sep-10-2007	Dec-11-2007	589.0	92
ALOS/PALSAR	515	FBS-FBS	A	Dec-11-2007	Jan-26-2008	406.3	46
ALOS/PALSAR	515	FBS-FBD	A	Jan-26-2008	Apr-27-2008	1175.9	92
ALOS/PALSAR	515	FBD-FBD	A	Apr-27-2008	Jun-12-2008	-6981.4	46
ALOS/PALSAR	515	FBD-FBD	A	Jun-12-2008	Jul-28-2008	3641.1	46
ALOS/PALSAR	515	FBD-FBS	A	Jul-28-2008	Dec-13-2008	-1178.6	138
ALOS/PALSAR	515	FBS-FBS	A	Dec-13-2008	Jan-28-2009	291.9	46
ALOS/PALSAR	515	FBS-FBD	A	Jan-28-2009	Jun-15-2009	675.4	138
ALOS/PALSAR	515	FBD-FBS	A	Jun-15-2009	Dec-16-2009	916.5	184
ALOS/PALSAR	515	FBS-FBS	A	Dec-16-2009	Jan-31-2010	608.8	46
ALOS/PALSAR	515	FBS-FBS	A	Jan-31-2010	Feb-03-2011	1795.9	368
ALOS/PALSAR	516	FBS-FBD	A	Feb-09-2007	Aug-12-2007	738.0	184
ALOS/PALSAR	516	FBD-FBD	A	Aug-12-2007	Sep-27-2007	172.7	46
ALOS/PALSAR	516	FBD-FBS	A	Sep-27-2007	Dec-28-2007	350.6	92
ALOS/PALSAR	516	FBS-FBD	A	Dec-28-2007	May-14-2008	1458.4	138
ALOS/PALSAR	516	FBD-FBD	A	May-14-2008	Jun-29-2008	-2819.6	46
ALOS/PALSAR	516	FBD-FBD	A	Jun-29-2008	Sep-29-2008	-1759.3	92
ALOS/PALSAR	516	FBD-FBS	A	Sep-29-2008	Nov-14-2008	473.5	46
ALOS/PALSAR	516	FBS-FBS	A	Nov-14-2008	Dec-30-2008	-41.5	46
ALOS/PALSAR	516	FBS-FBS	A	Dec-30-2008	Feb-14-2009	740.5	46
ALOS/PALSAR	516	FBS-FBS	A	Feb-14-2009	Aug-17-2009	386.1	184
ALOS/PALSAR	516	FBS-FBD	A	Aug-17-2009	Oct-02-2009	547.3	46
ALOS/PALSAR	516	FBD-FBS	A	Oct-02-2009	Jan-02-2010	529.0	92
ALOS/PALSAR	516	FBS-FBS	A	Jan-02-2010	Feb-20-2011	2494.0	414
TSX/SAR	113	StripMap 007R	A	May-08-2012	Jun-10-2012	-366.3	33
TSX/SAR	113	StripMap 007R	A	Jun-10-2012	Jun-21-2012	332.7	11
TSX/SAR	113	StripMap 007R	A	Jun-21-2012	Nov-11-2012	5.9	143
TSX/SAR	113	StripMap 007R	A	Nov-11-2012	Apr-14-2013	-122.6	154
TSX/SAR	113	StripMap 007R	A	Apr-14-2013	May-06-2013	-377.6	22
TSX/SAR	113	StripMap 007R	A	May-06-2013	Oct-07-2013	-48.6	154
TSX/SAR	113	StripMap 007R	A	Oct-07-2013	Oct-18-2013	248.5	11
TSX/SAR	113	StripMap 007R	A	Oct-18-2013	Oct-29-2013	-157.6	11
TSX/SAR	113	StripMap 007R	A	Oct-29-2013	Nov-09-2013	114.9	11
TSX/SAR	113	StripMap 007R	A	May-04-2014	May-15-2014	301.0	11
TSX/SAR	113	StripMap 007R	A	May-15-2014	May-26-2014	-68.7	11
TSX/SAR	113	StripMap 007R	A	May-26-2014	Jun-06-2014	110.7	11
TSX/SAR	113	StripMap 007R	A	Jun-06-2014	Jun-17-2014	139.5	11
TSX/SAR	166	StripMap 006R	D	Nov-26-2012	Apr-07-2013	-189.4	132
TSX/SAR	166	StripMap 007R	D	Nov-15-2012	Mar-27-2013	115.7	132
TSX/SAR	166	StripMap 008R	D	Oct-24-2012	Dec-18-2012	-80.0	55
TSX/SAR	166	StripMap 009R	D	Oct-13-2012	Dec-07-2012	123.6	55
TSX/SAR	166	StripMap 009R	D	Dec-07-2012	Apr-18-2013	38.0	132
TSX/SAR	166	StripMap 009R	D	Apr-18-2013	Sep-30-2013	-366.7	165
TSX/SAR	166	StripMap 009R	D	Sep-30-2013	Oct-22-2013	259.7	22
TSX/SAR	166	StripMap 009R	D	Oct-22-2013	May-08-2014	78.9	198
TSX/SAR	166	StripMap 009R	D	May-08-2014	May-30-2014	140.0	22
TSX/SAR	166	StripMap 009R	D	May-30-2014	Jun-10-2014	-184.2	11
TSX/SAR	166	StripMap 009R	D	Jun-10-2014	Sep-28-2014	-45.7	110
TSX/SAR	166	StripMap 009R	D	Sep-28-2014	Oct-09-2014	7.3	11

3.3.2 Glacier terminus position and visible surge features

Landsat imageries

Landsat (LSAT) satellites are one of the longest earth observation missions operated by NASA since 1972. The multispectral scanner (MSS) onboard LSAT 1, 2 and 3 operated from 1972 to 1983 had four spectral bands ranging from visible green to the near-infrared (NIR) wavelengths with the ground resolution of ~80 m. The imageries with the thematic mapper (TM) onboard LSAT 4 and 5 are available from 1982 to 2013, in which the sensor comprises six bands ranging from visible blue to IR with an improved spatial resolution of 30 m and one thermal band with the resolution of 120 m. LSAT 7 carried the enhanced thematic mapper plus (ETM+) which consists of the six bands similar to TM sensor, one thermal band with the improved resolution of 60m and additional panchromatic band with the resolution of 15 m. Imageries with LSAT 7 are available from 1999. However, the failure of the scan line corrector caused the data gap on imageries from May 2003. LSAT 8 launched on February 2013 carrying the operational land imager and thermal infrared sensor (OLI/TIRS) composed of 11 spectral bands including additional two bands and the refined 9 bands with spatial resolution from 15 m of panchromatic to 100 m of TIRS band.

A box measurement method

To detect changes in glacier terminus position, I used a box measurement method [Moon and Joughin, 2008], following the processing method by McNabb and Hock

[2014] who manually digitalized terminus outlines using false color images composed of different bands through LSAT 1 to 7. In addition, I used SAR intensity imageries and LSAT8 OLI/TIRS imageries. The combination of color images for each sensor is shown in Table 3.3. I manually delineated a centerline and terminus outlines for the 31 glaciers and 2 separated branches in WKS with QGIS software (http://www.qgis.org) (Fig. 3.3).

Visible surge features

True color imageries were used to detect visible surge features including elongated or looped moraines by the past surge activity, propagation of surge front marked by the bulge and the completely crevassed surface [Jiskoot, 2011]. Composition of bands for each sensor was listed in table 3.3. Note that imageries from MSS sensor were composed with a false color because the sensor did not cover blue in spectrum.

Table 3.3: Landsat sensor spec table

Sensor platform	MSS LSAT1-3	TM and ETM+ LSAT4-5, and LSAT7	OLI/TIRS LSAT8
		band designations (μm)	
band1	-	blue (0.45-0.52)	CA (0.43-0.45)
band2	-	green (0.52-0.60)	blue (0.45-0.51)
band3	-	red (0.63-0.69)	green (0.53-0.59)
band4	green (0.5-0.6)	NIR (0.77-0.90)	red (0.64-0.67)
band5	red (0.6-0.7)	SWIR (1.55-1.75)	NIR (085.-0.88)
band6	NIR (0.7-0.8)	TIRS (10.40-12.50)	SWIR (1.57-1.65)
band7	NIR (0.8-1.1)	SWIR(2.09-2.35)	SWIR (2.11-2.29)
band8	-	Pan (0.52-0.90) [b]	Pan (.50-.68)
band9	-	-	Cirrus (1.36 -1.38)
band10	-	-	TIRS (10.60-11.19)
band11	-	-	TIRS (11.5-12.51)
spatial resolution	nominal 60 m [a]	nominal 30m TIRS : 120m/60m [b] Pan : 15 m	nominal 30m TIRS : 100m Pan : 15m
		composed bands (Red, Green, Blue)	
true color	-	(b3, b2, b1)	(b4, b3, b2)
false color	(b6, b5, b4)	(b5, b4, b3)	(b7, b5, b1)

a: MSS pixel size is resampled from original 79 x 57 meters
b: ETM+only.
NIR : Near Infrared, SWRI : short-wave Infrared, TIRS : thermal Infrared, CA : coastal aerosol, Pan : panchromatic

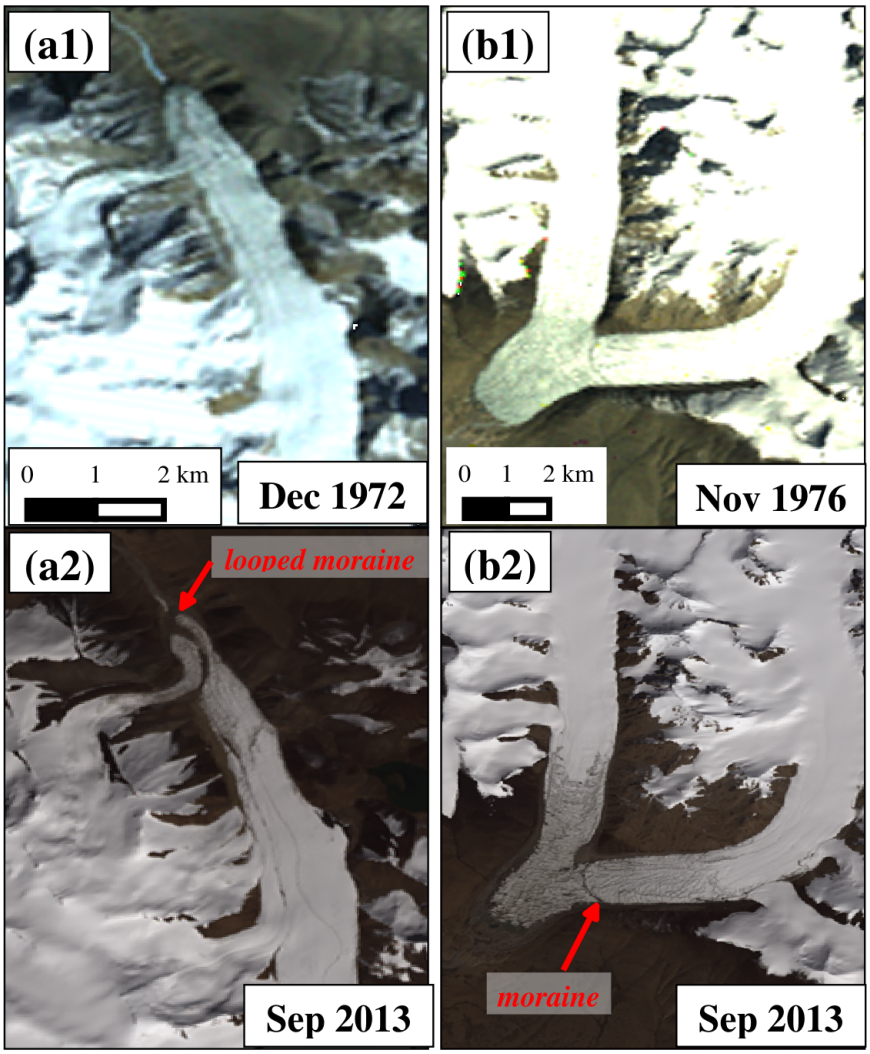

Figure 3.2: Moraine structure indicative of past surging in WKS. Yake glacier at Dec 1972 (a1) and at Sep 2013. Gongxing glacier at Nov 1976 (b1) and at Sep 2013 (b2).

Table 3.4: Landsat data table

Sensor	path	row	date (yyyymmdd)	Sensor	path	row	date (yyyymmdd)
L1-3 MSS	156	35-36	19721201	L7 ETM	145	36	19990929
	156	35-36	19761101	(slc-on)	145	35	19991031
	156	35-36	19761119		145	35	19991218
	156	35-36	19770729		145	36	20000103
L4-5 TM	145	35	19890120		145	35-36	20000510
	145	35	19901115		145	35	20000627
	145	36	19911017		145	35	20001017
	145	35-36	19981004		145	35-36	20001204
	145	35	20061010	L7 ETM	145	35-36	20030722
	145	35-36	20070506	(slc-off)	145	35-36	20031127
	145	35-36	20070810		145	35-36	20040302
	145	36	20070927		145	36	20050201
	145	36	20090103	L8 OLI	145	35-36	20130522
	145	35-36	20090204		145	35-36	20130607
	145	35-36	20090308		145	35-36	20130623
	145	35-36	20090324		145	35-36	20130709
	145	35-36	20090815		145	35-36	20130725
	145	35-36	20091002		145	35-36	20130810
	145	35-36	20091103		145	35-36	20130911
	145	35-36	20100122		145	35-36	20130927
	145	35-36	20100311		145	35-36	20131130
	145	35	20100412		145	35-36	20131216
	145	35-36	20100717		145	35-36	20140202
	145	35-36	20101106		145	35-36	20140218
	145	35-36	20101208		145	35-36	20140322
	145	35-36	20110125		145	35-36	20140423
	145	35-36	20110210		145	35-36	20140509
	145	35-36	20110314		145	35-36	20140525
	145	35-36	20110415				
	145	35-36	20110501				
	145	35-36	20110805				
	145	35-36	20111024				
	145	35-36	20111109				

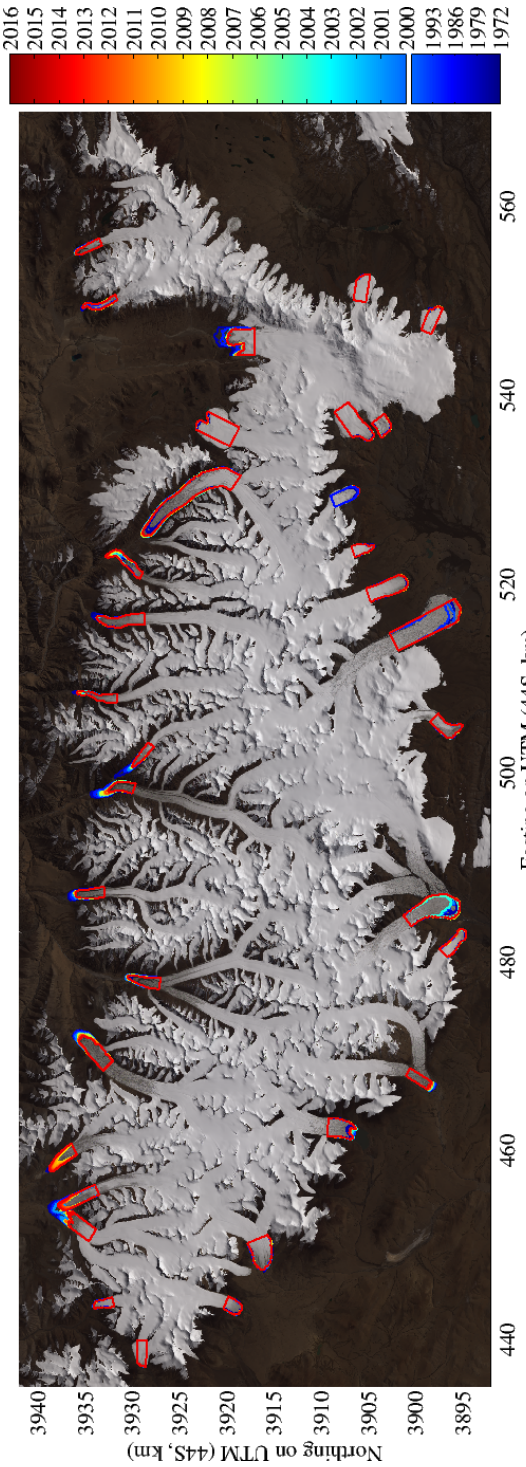

Figure 3.3: Setting of terminus polygons in a box measurement method

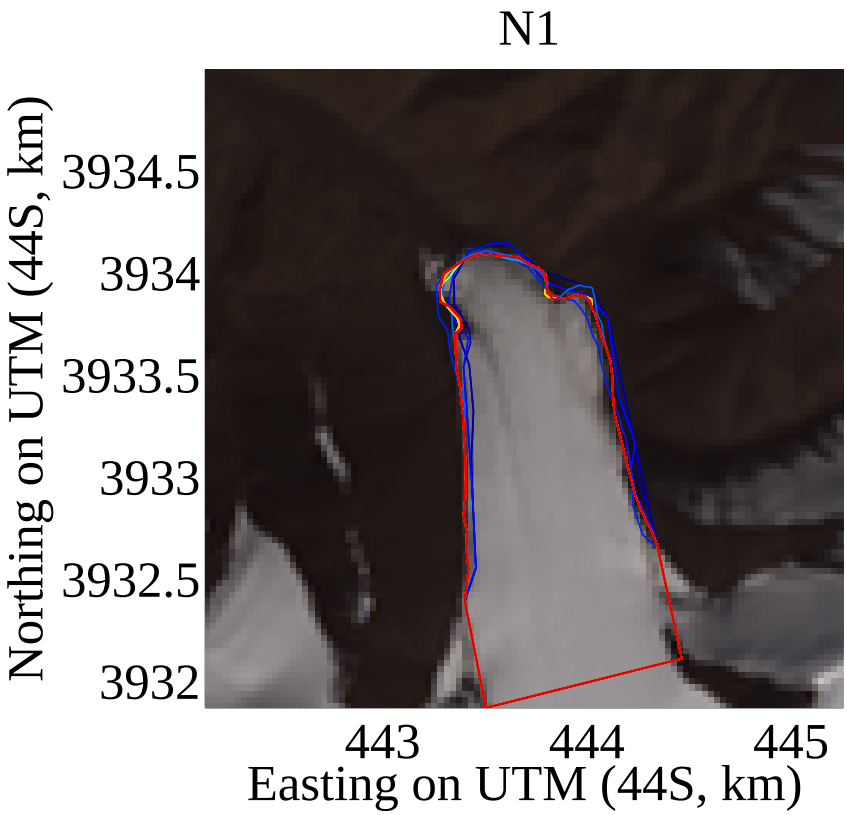

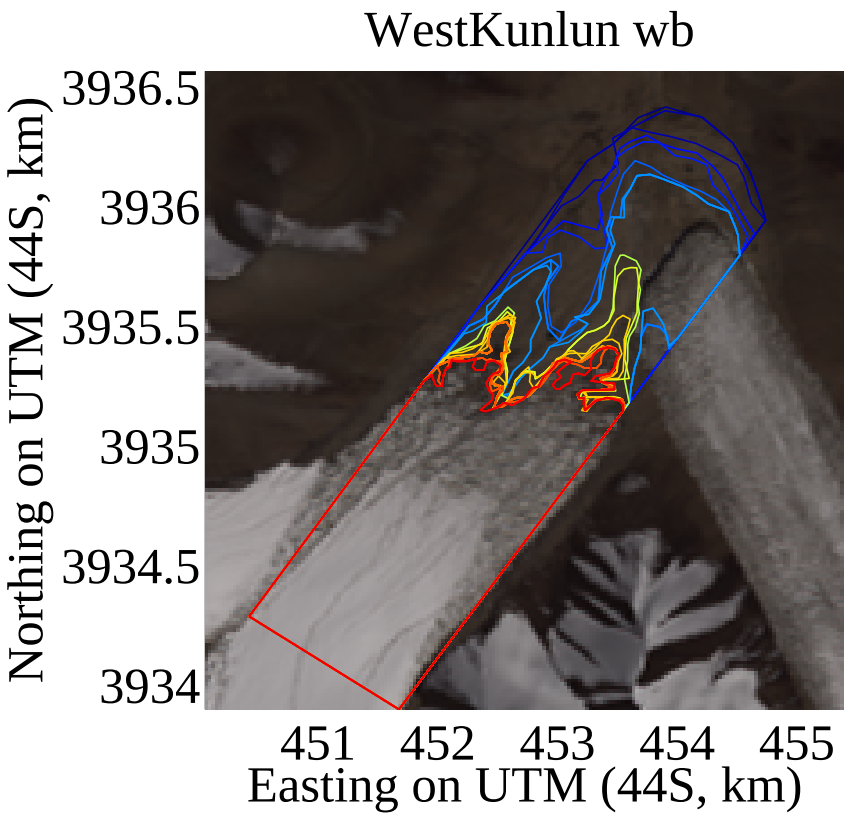

Figure 3.3: (continued) Setting of terminus polygons in a box measurement method

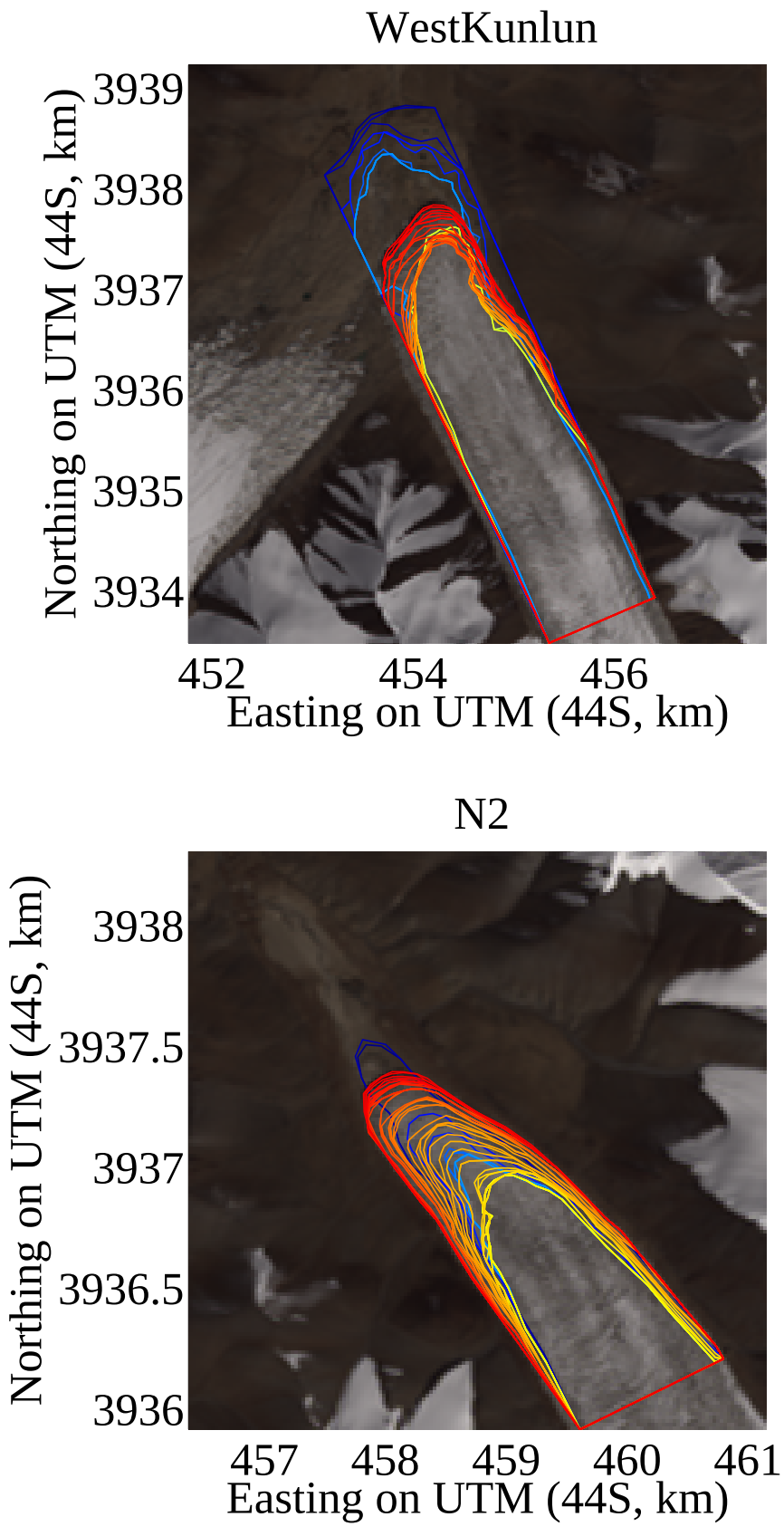

Figure 3.3: (continued) Setting of terminus polygons in a box measurement method

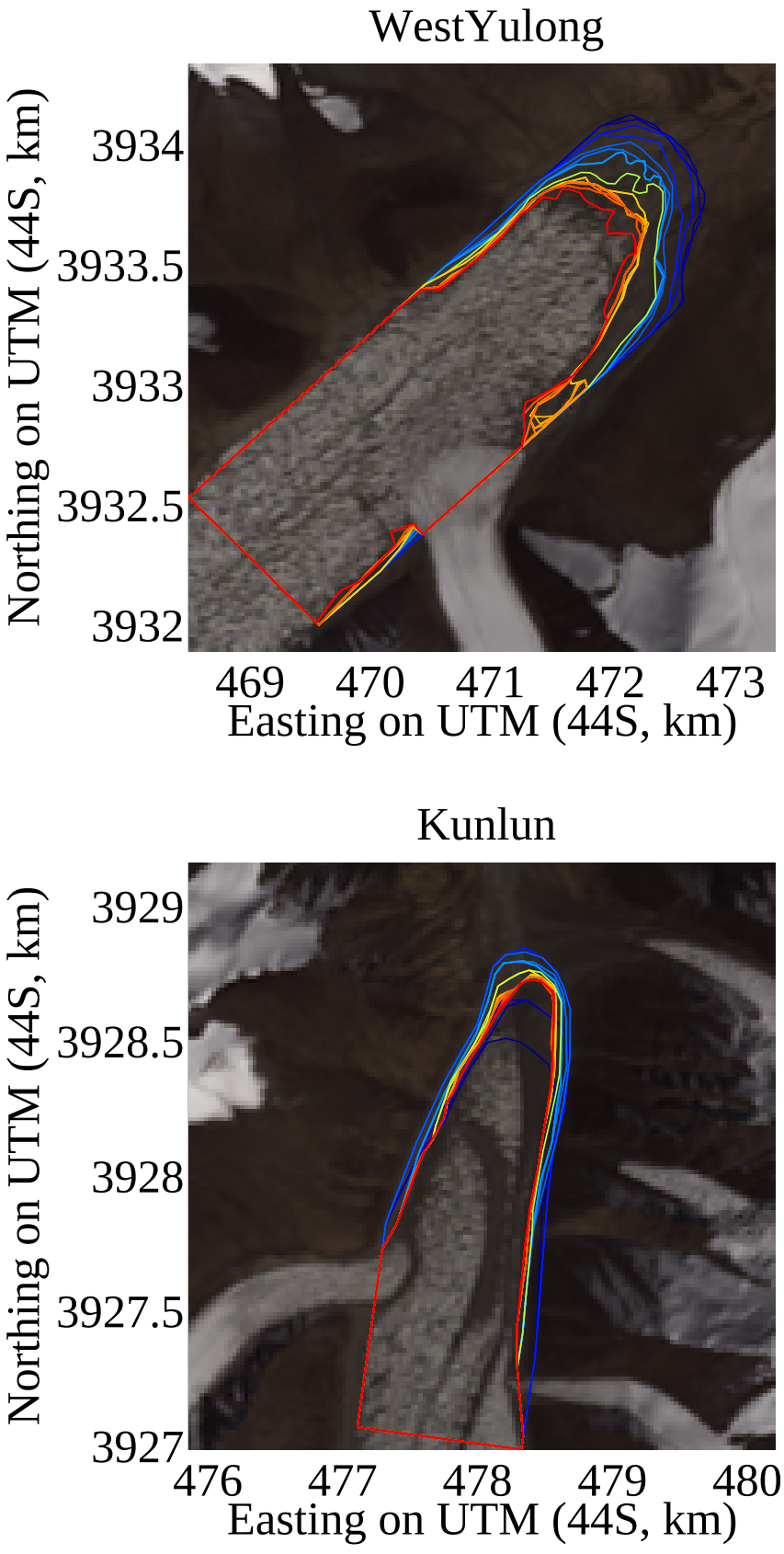

Figure 3.3: (continued) Setting of terminus polygons in a box measurement method

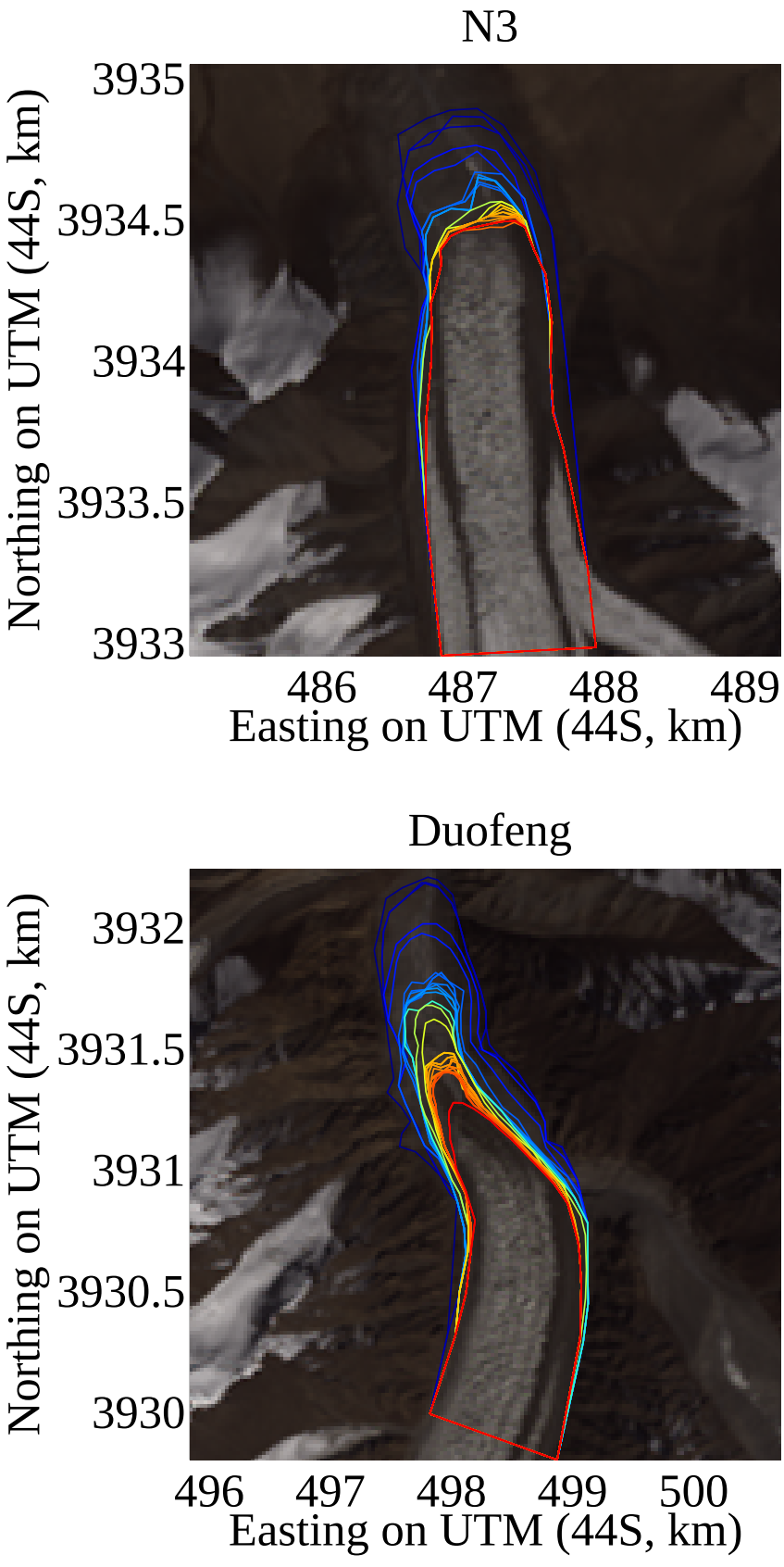

Figure 3.3: (continued) Setting of terminus polygons in a box measurement method

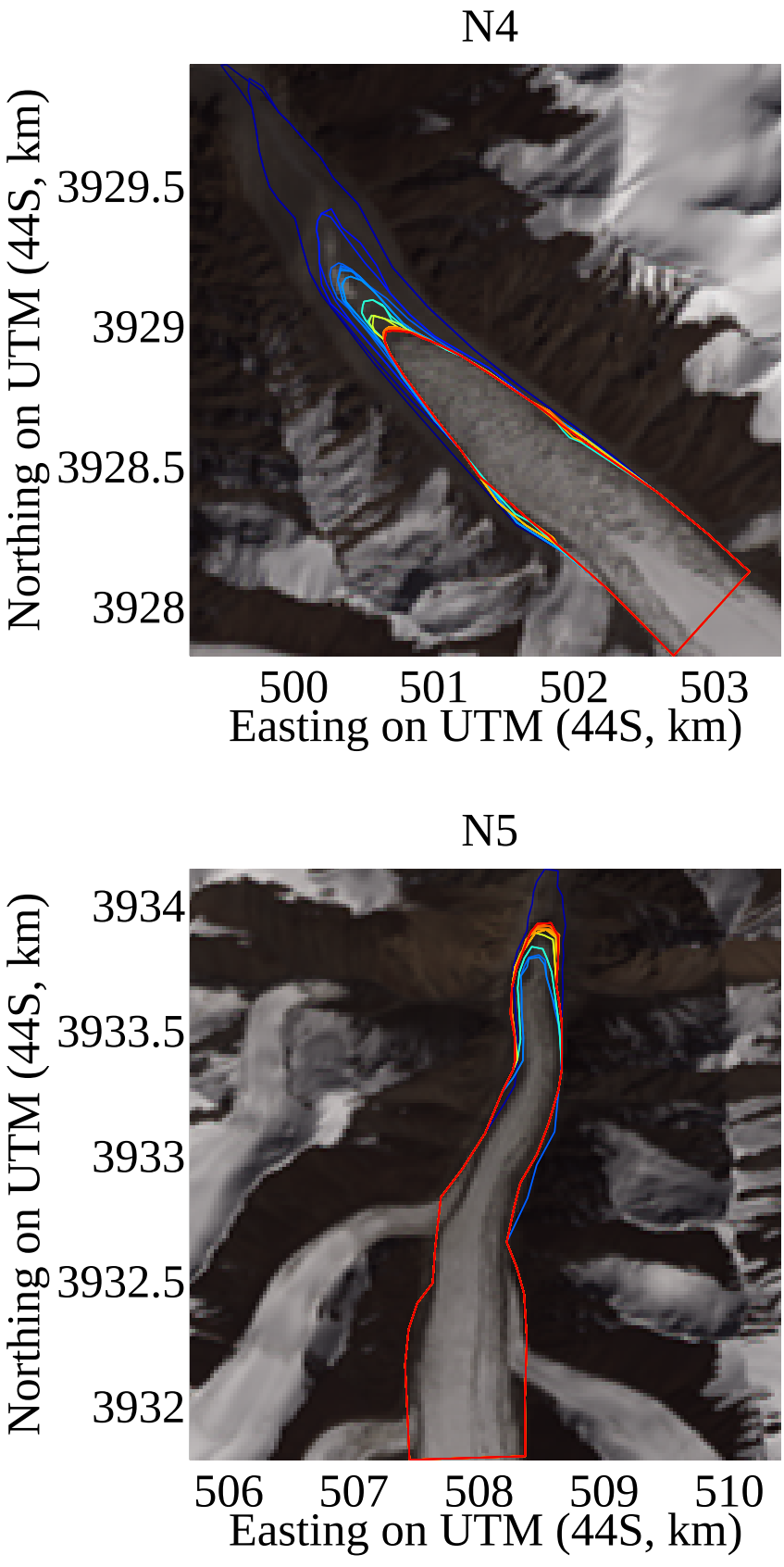

Figure 3.3: (continued) Setting of terminus polygons in a box measurement method

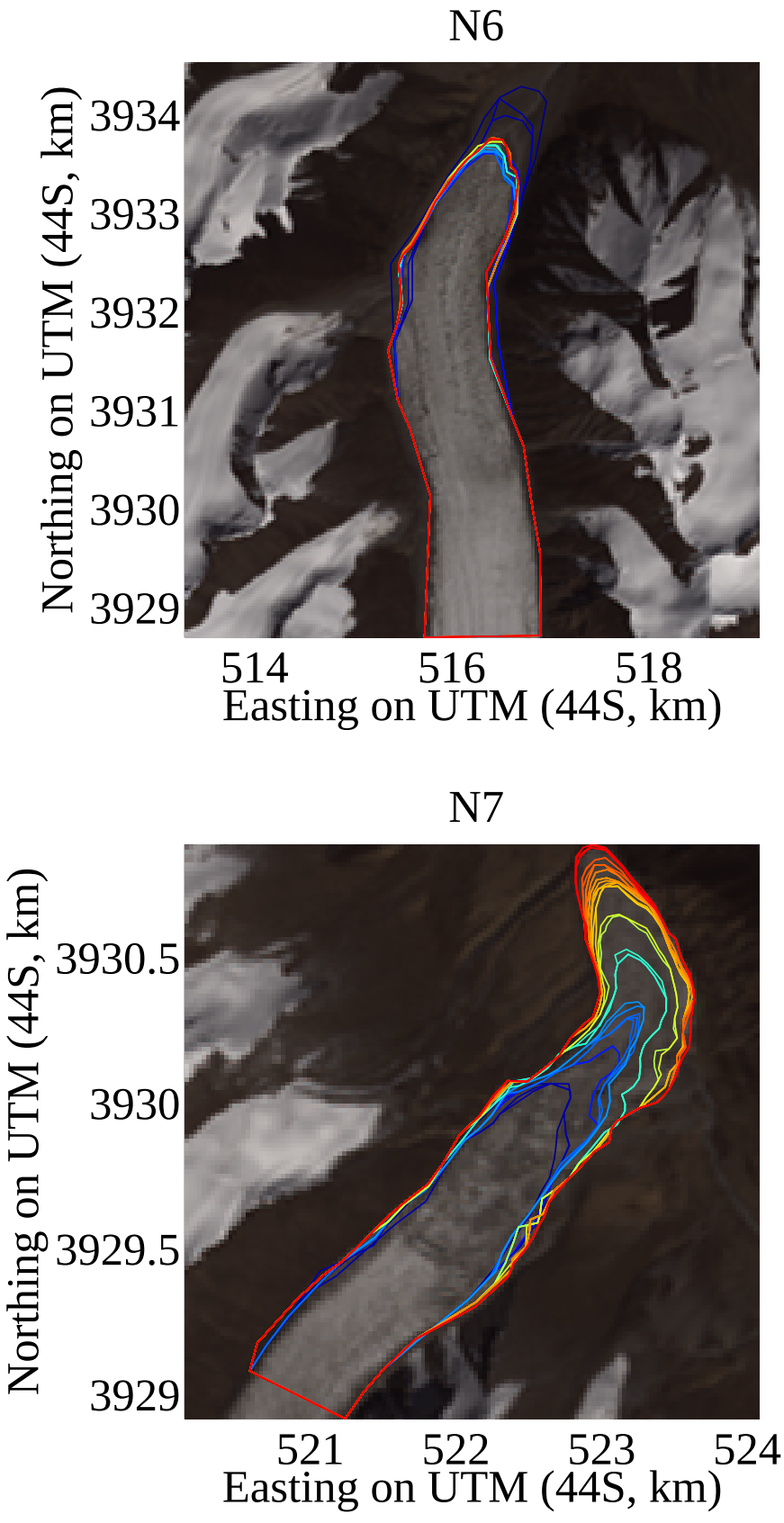

Figure 3.3: (continued) Setting of terminus polygons in a box measurement method

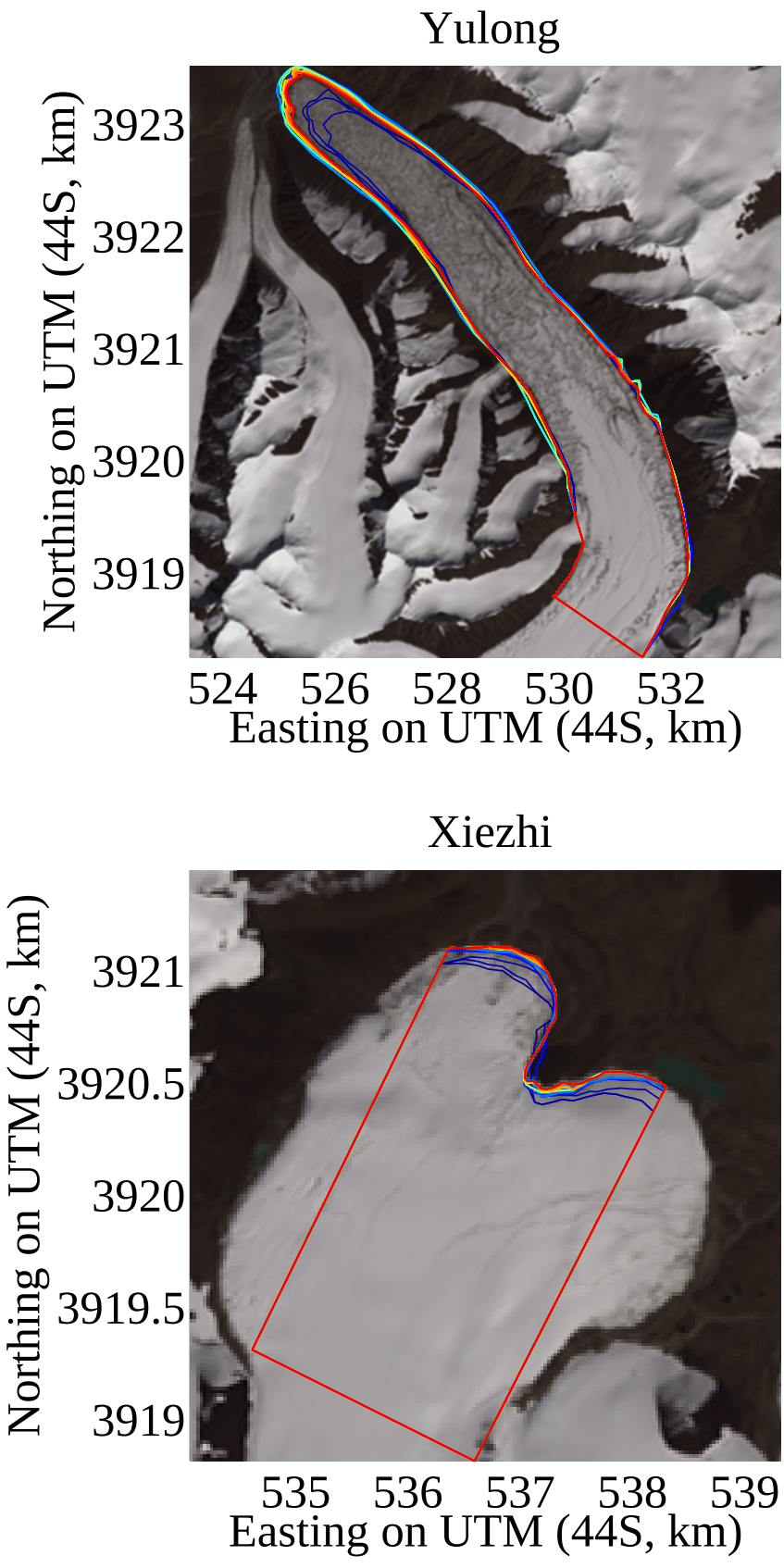

Figure 3.3: (continued) Setting of terminus polygons in a box measurement method

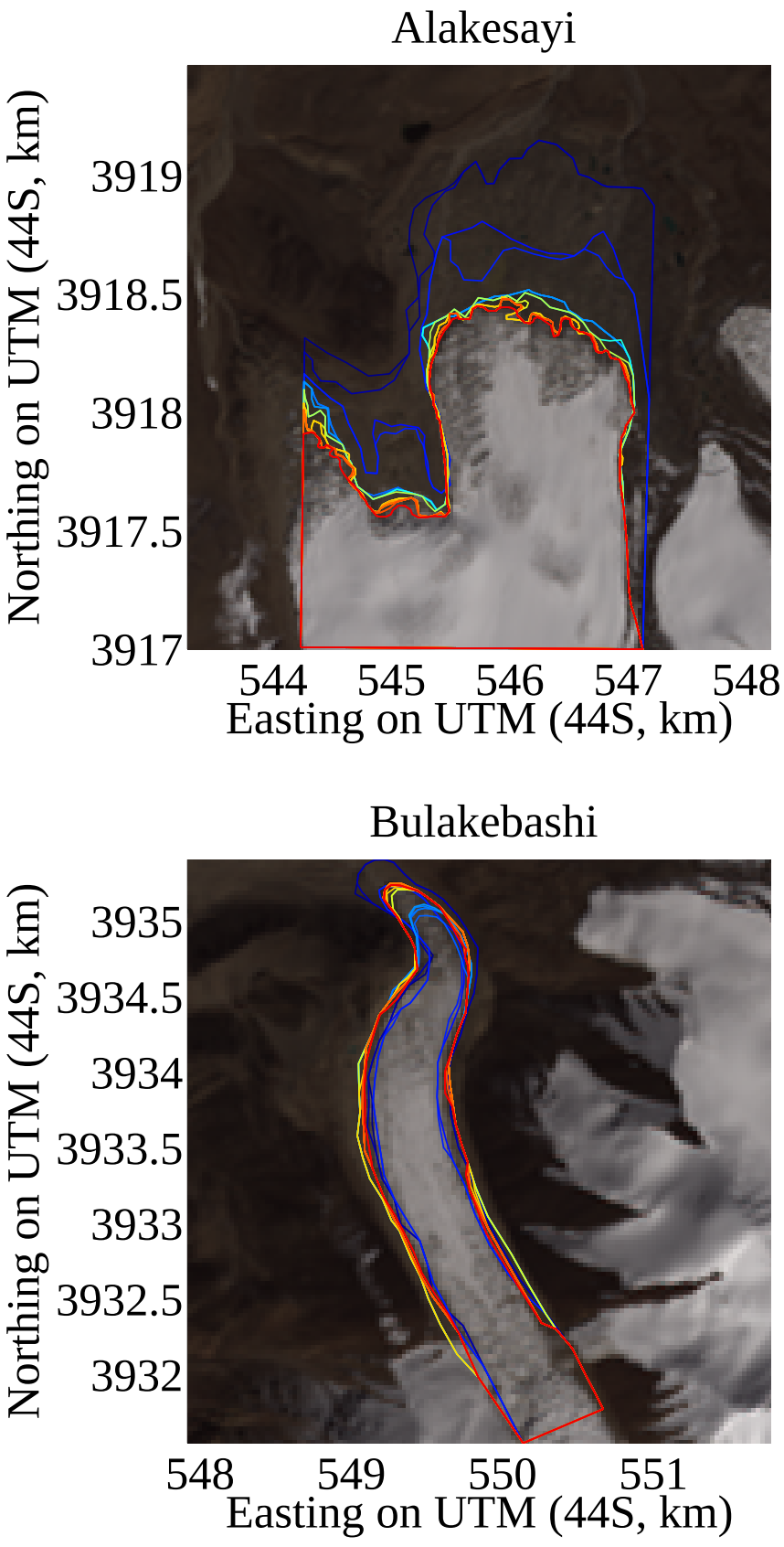

Figure 3.3: (continued) Setting of terminus polygons in a box measurement method

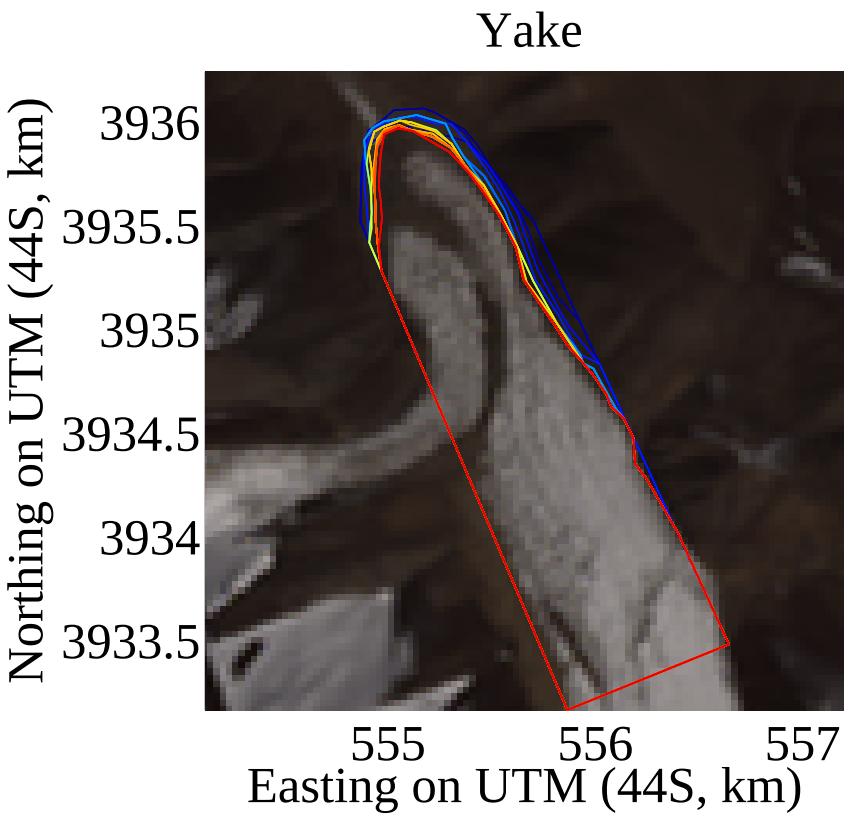

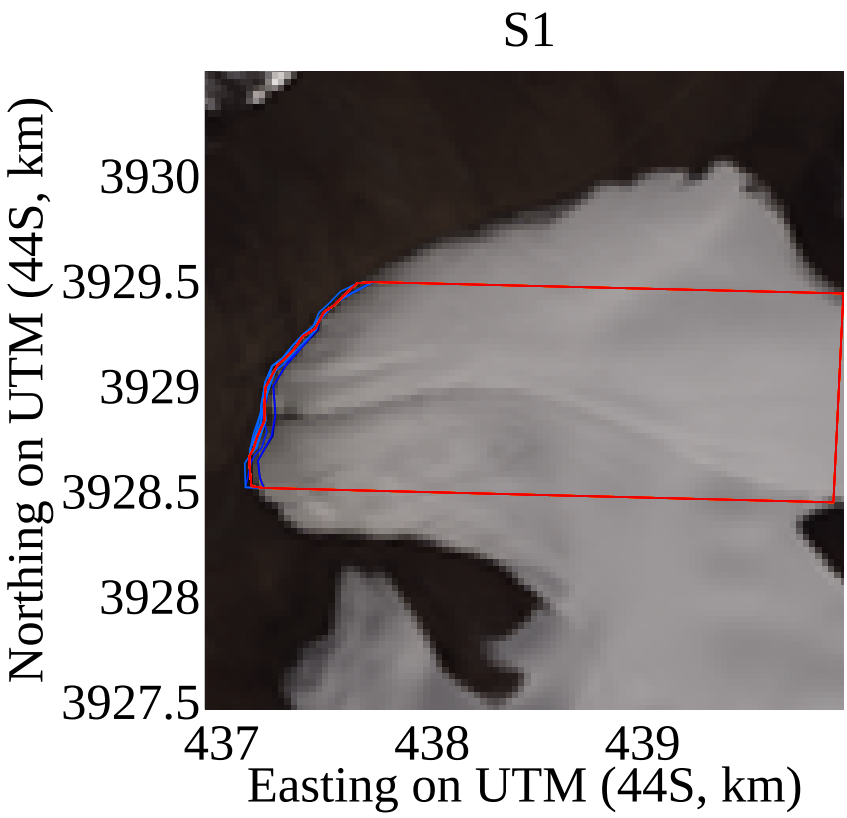

Figure 3.3: (continued) Setting of terminus polygons in a box measurement method

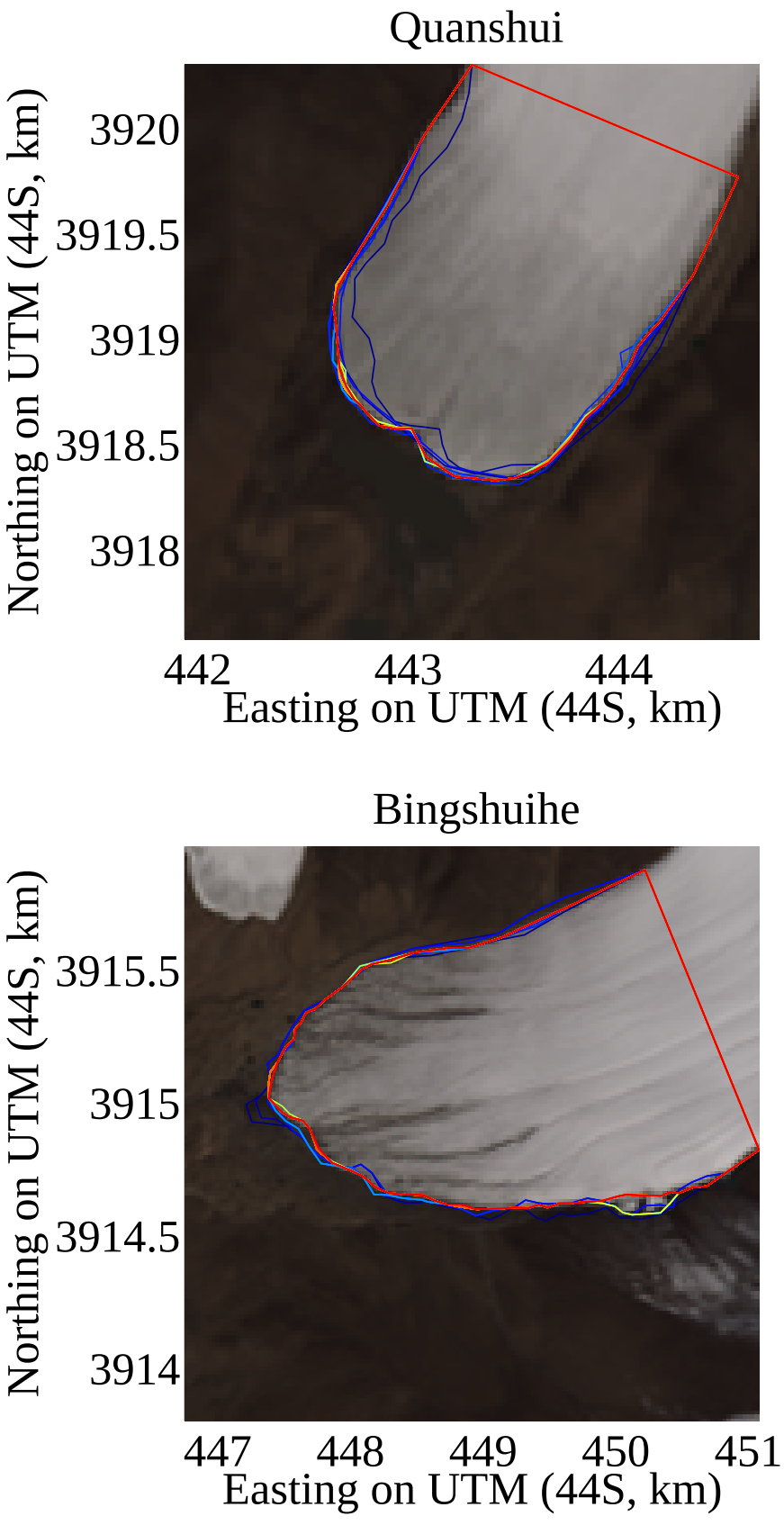

Figure 3.3: (continued) Setting of terminus polygons in a box measurement method

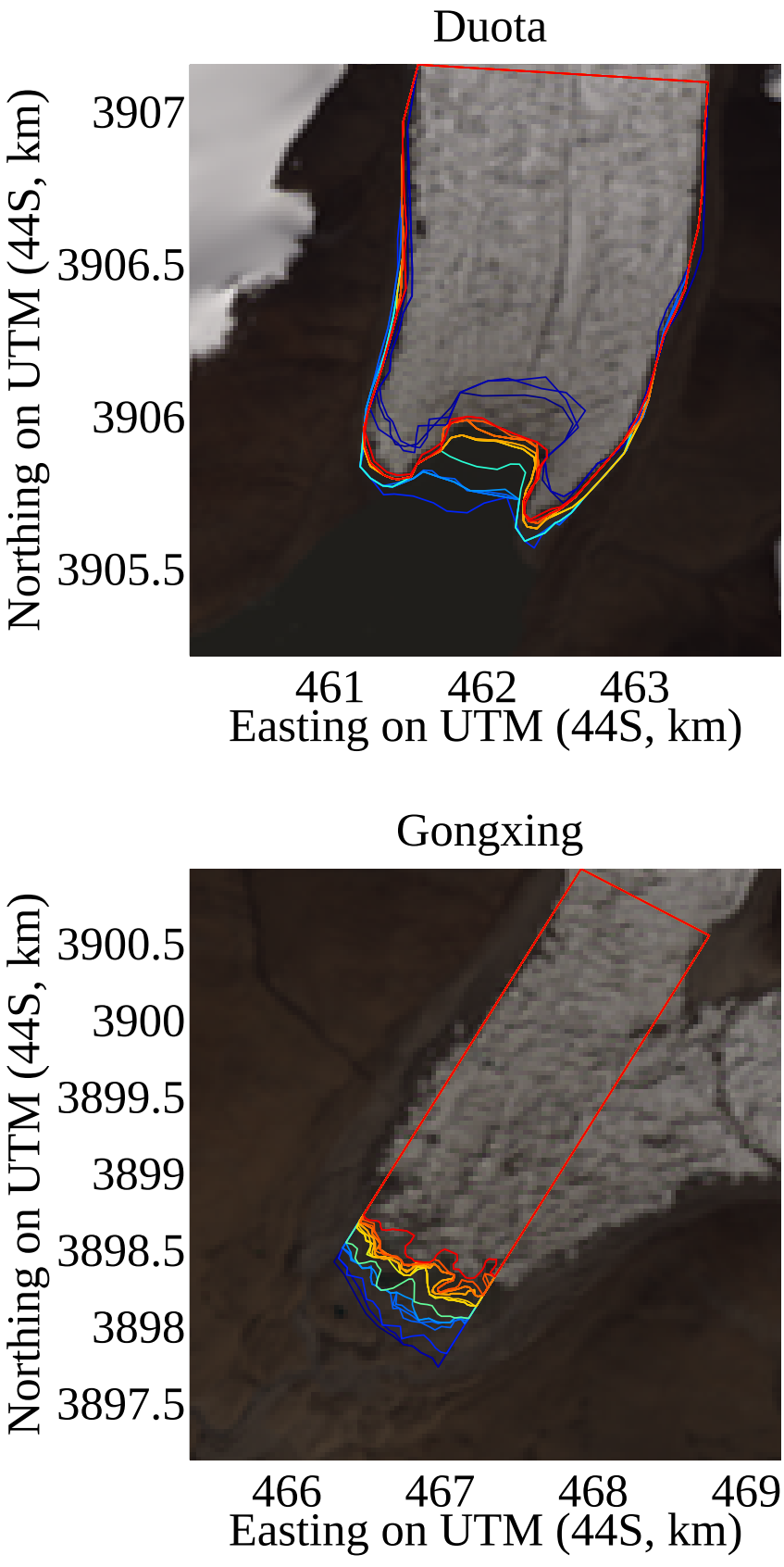

Figure 3.3: (continued) Setting of terminus polygons in a box measurement method

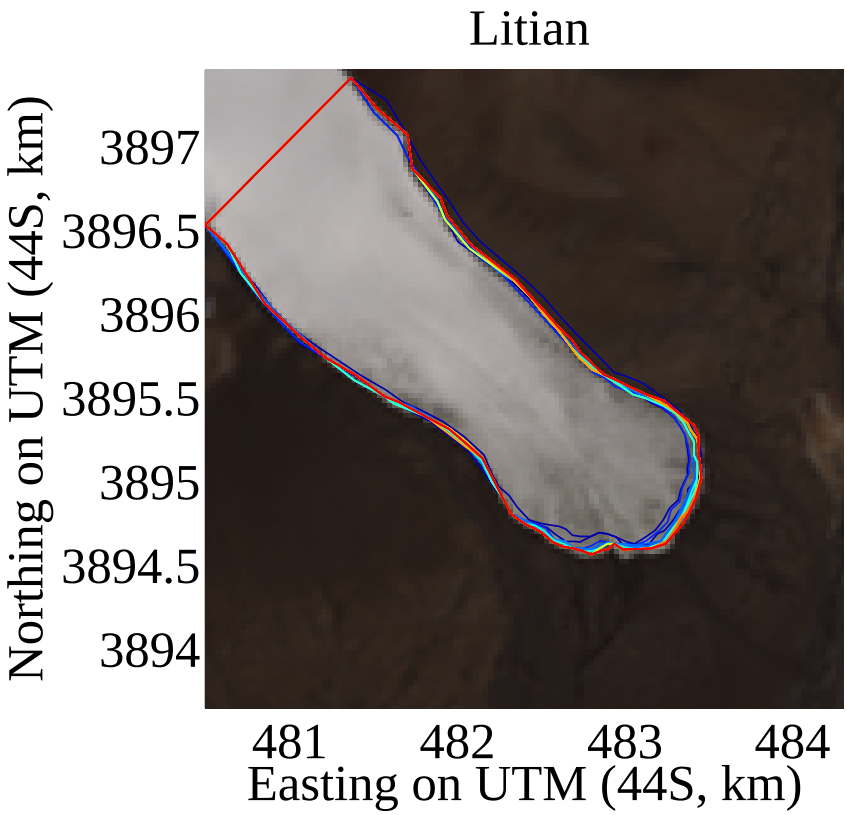

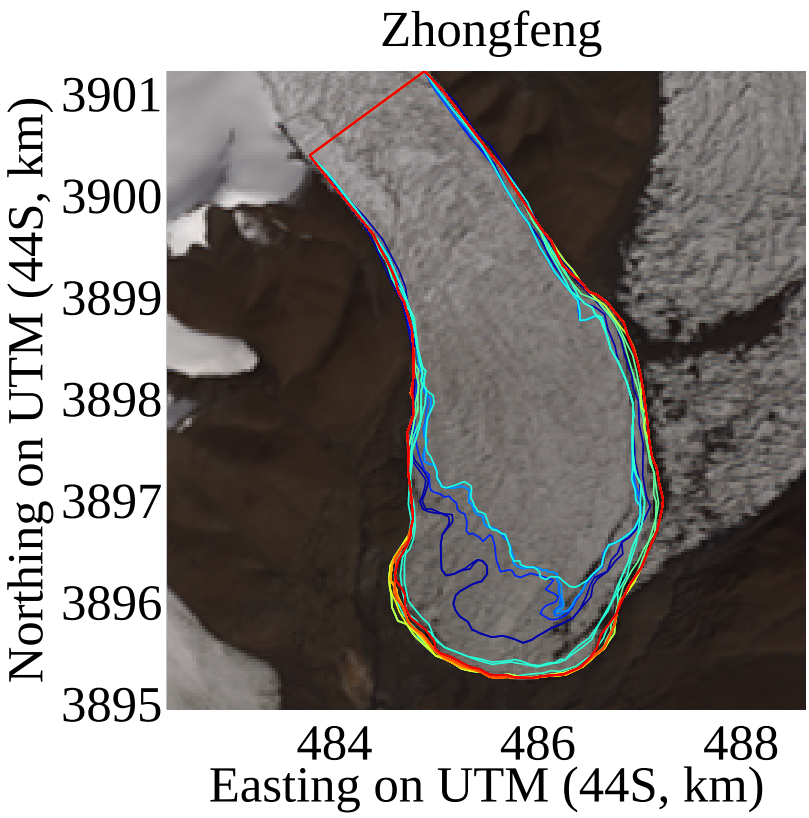

Figure 3.3: (continued) Setting of terminus polygons in a box measurement method

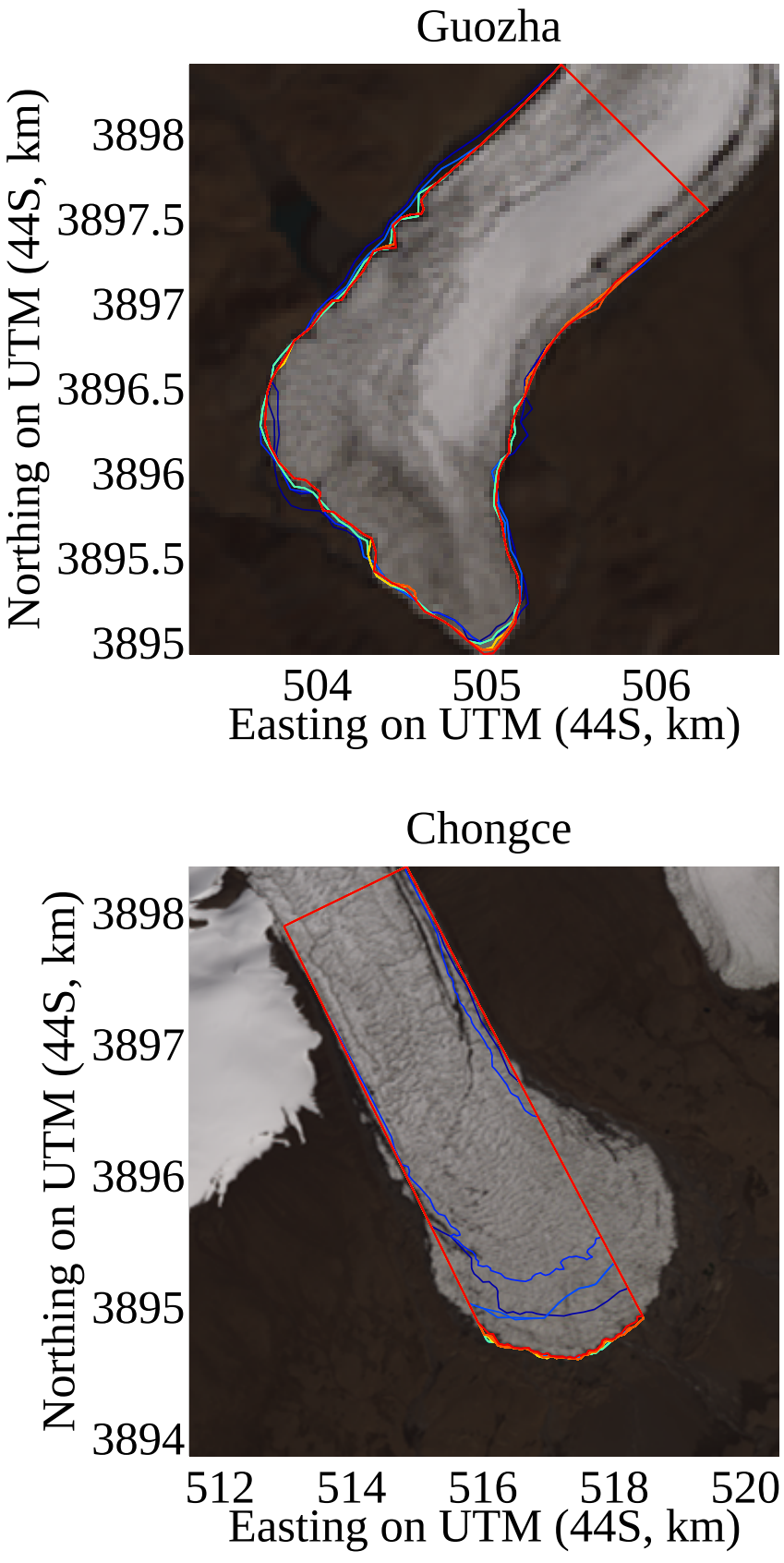

Figure 3.3: (continued) Setting of terminus polygons in a box measurement method

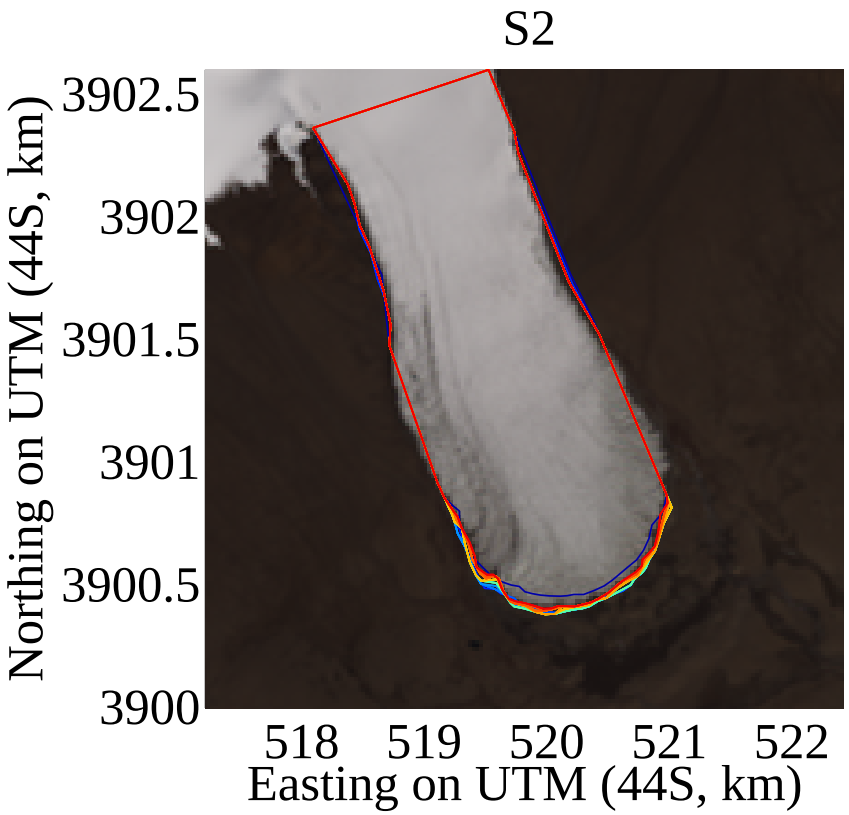

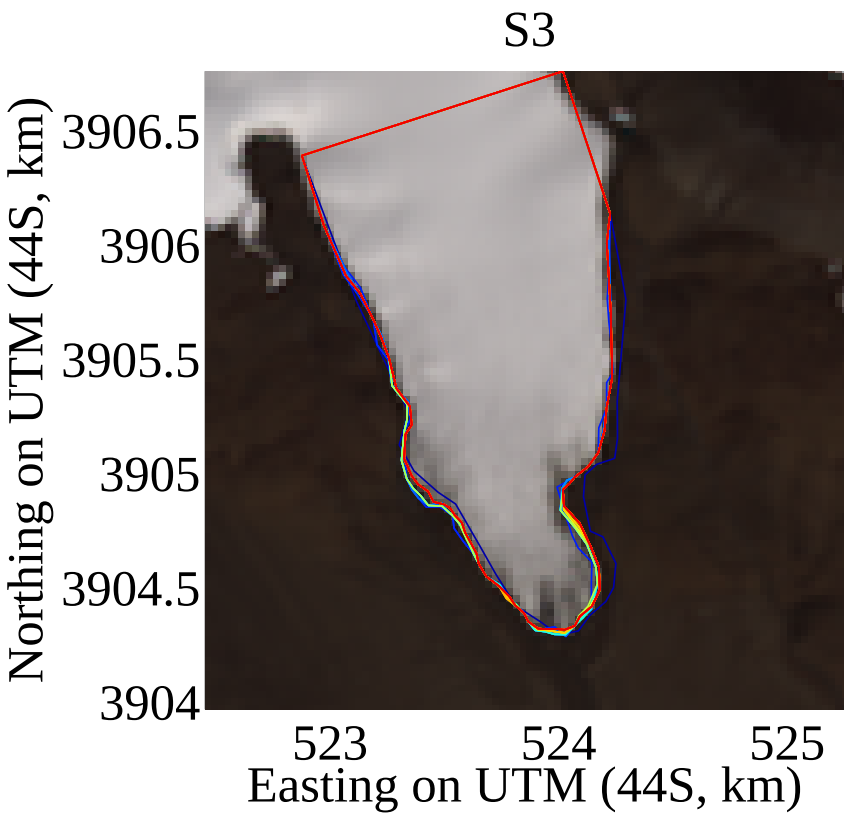

Figure 3.3: (continued) Setting of terminus polygons in a box measurement method

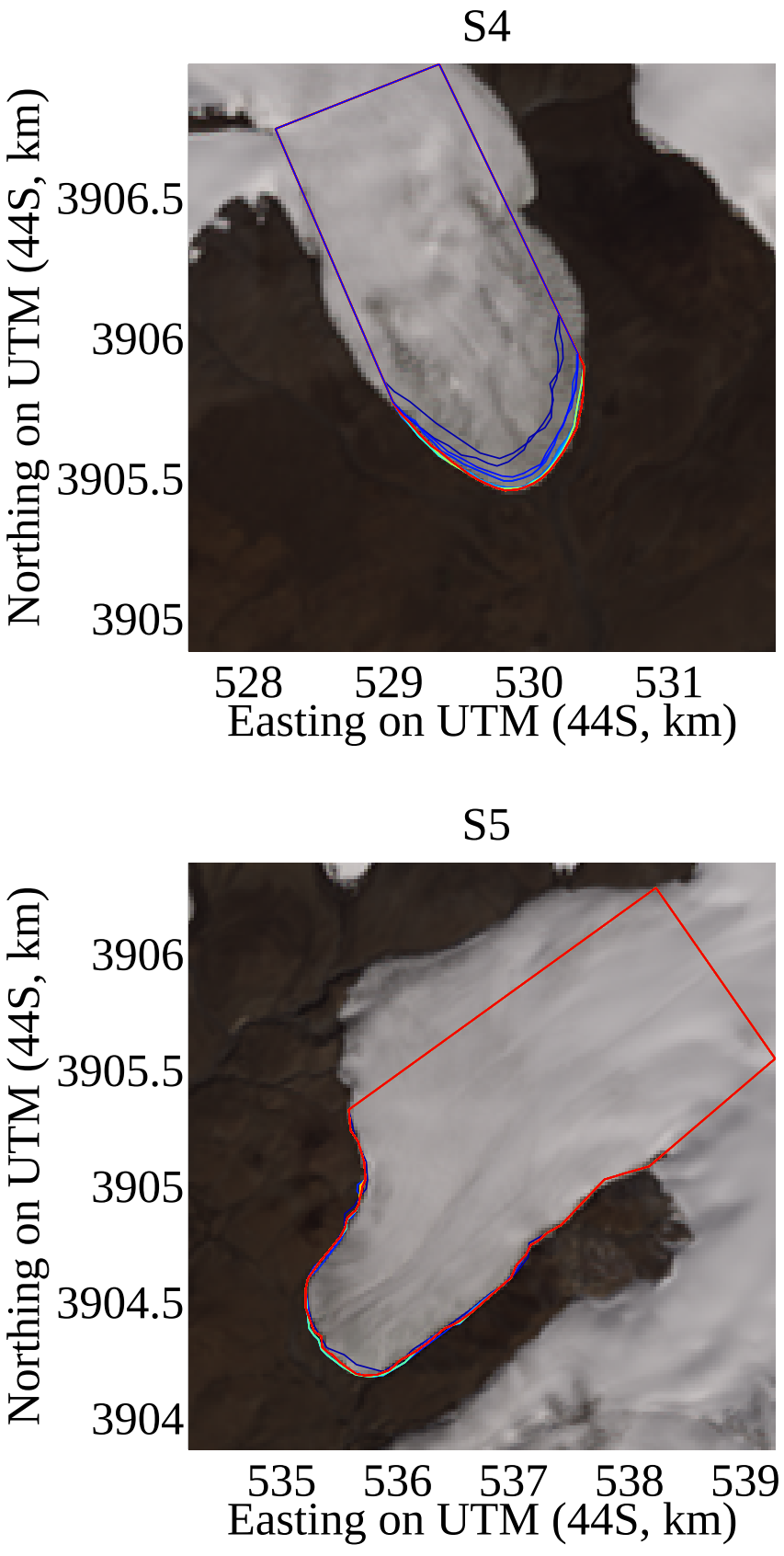

Figure 3.3: (continued) Setting of terminus polygons in a box measurement method

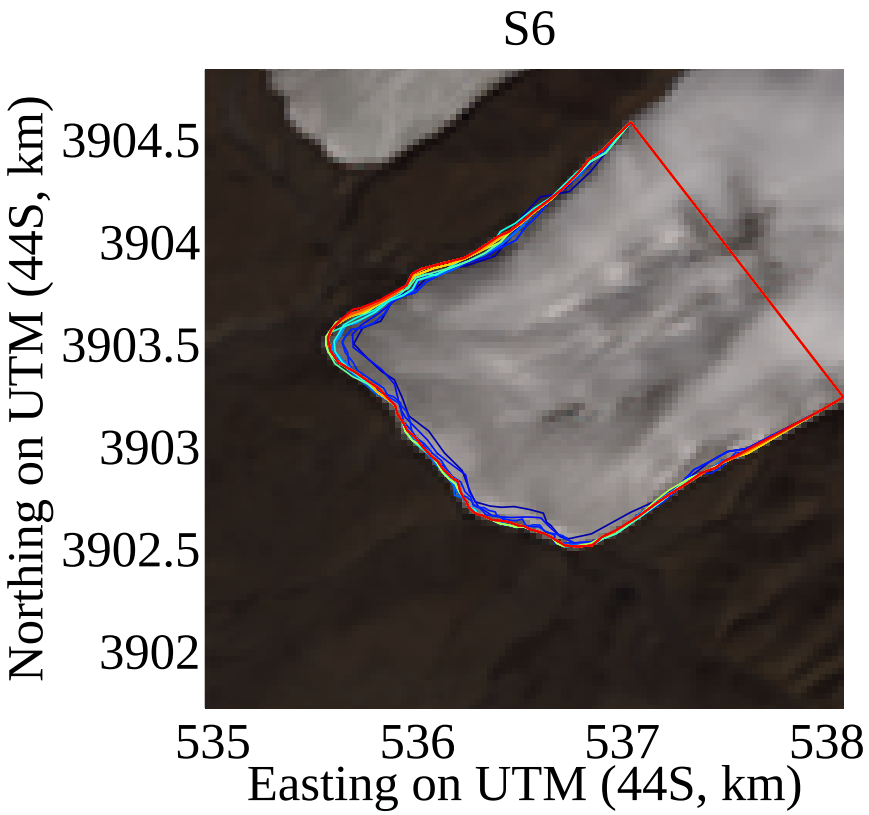

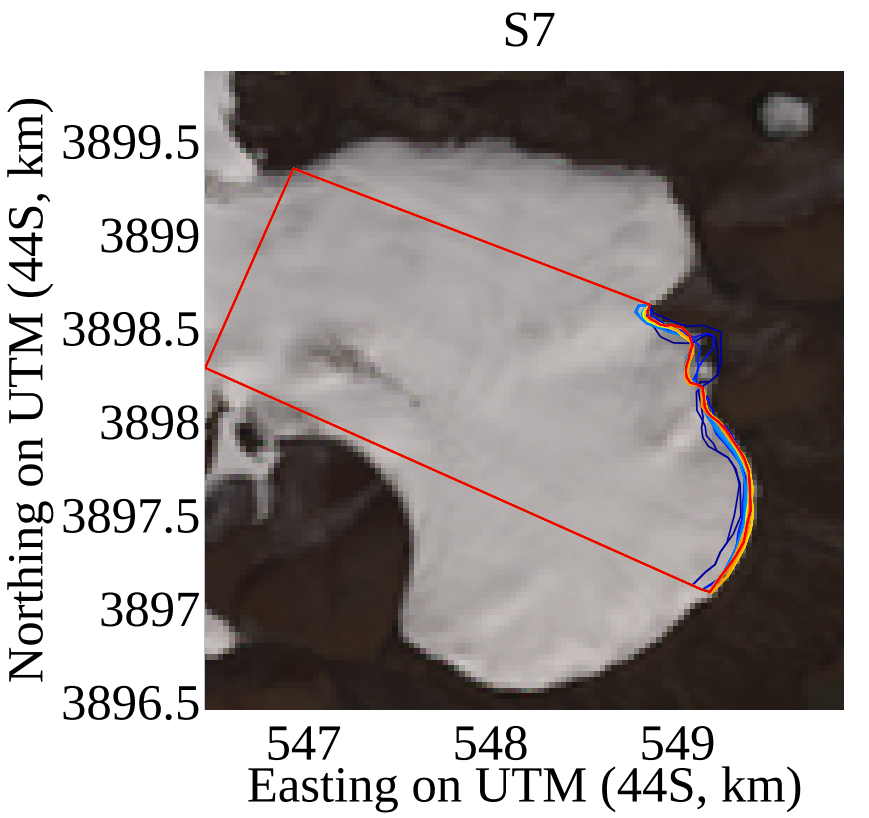

Figure 3.3: (continued) Setting of terminus polygons in a box measurement method

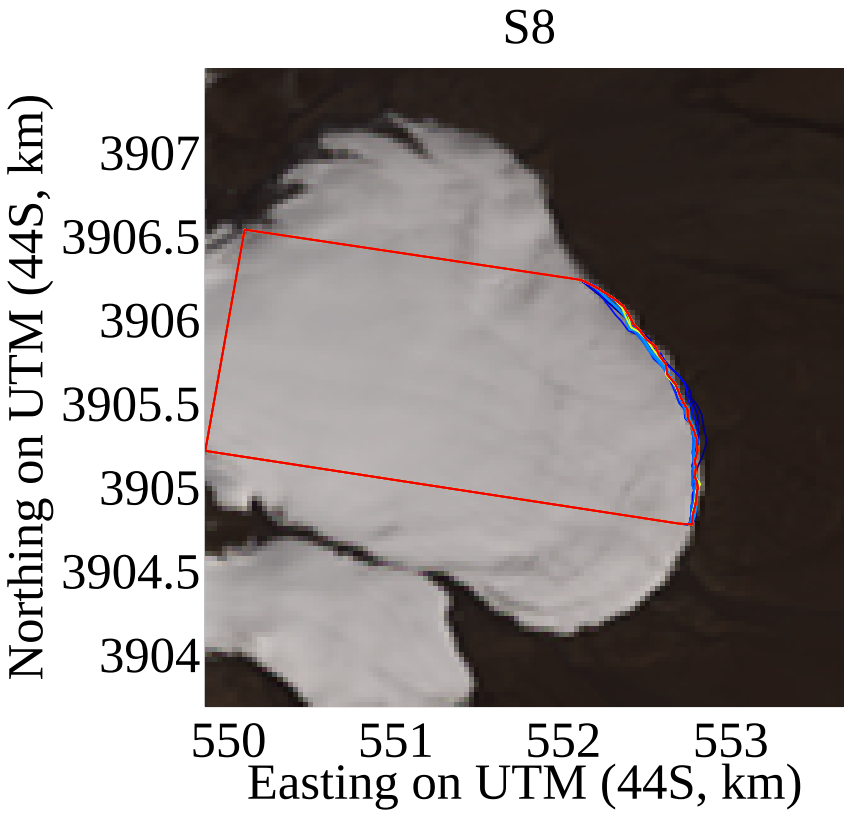

Figure 3.3: (continued) Setting of terminus polygons in a box measurement method

3.3.3 The criteria to identify surge-type glaciers

The criteria to identify surge-type glaciers in the WKS are not straightforward, because the fore-mentioned satellite remote sensing imageries are not homogeneous in terms of both the measurement datasets and their spatial-temporal resolutions. Furthermore almost debris-free glaciers in WKS do not clearly preserve the indicative of past surging. Surging glaciers in WKS can be easily identified from surging velocity, surge front propagation and rapid advance in their terminus position with heavily surface crevassing [Yasuda and Furuya, 2013]. On the other hand, surge-type glaciers in quiescent phase are necessary to inspect carefully, because some surge features also appear on normal glacier, for example crevassed surface, retreating and stagnant flow, also appear on normal glaciers. Also, it is difficult to distinguish surge-type from normal glacier if there was no distinctive feature like looped moraine. Therefore, I classified glaciers into three categories: surge-type glacier, uncertain and non-surge glacier. Note that the second one could be classified into the surge-type by further investigations.

3.4 Results and discussions

I investigated 31 glaciers in West Kunlun Shan from 1972 to 2014 and identified 11 surge-type glaciers. The 5 surge-type glaciers experienced an active phase in which flow speed exceeded ~200m/year with advancing in its terminus position and heavily crevassing during SAR observation period since 1992. The 4 glaciers showed surge features and advanced between 1972-1992. The 2 glaciers did not show surging behavior during our observation period but had looped moraine and the other surge features. I describe in detail below how I considered each glacier as surge type, and the results are summarized in Table 3.5. I was not able to distinguish between surge-type and non-surge-type for the 6 glaciers whose terminus position changed rapidly. The others 14 glaciers showed no surge features and their terminus position were almost static.

Table 3.5: Surge glaciers and detected surge features

Glacier Name	RGIID	Surge features
Northern slope		
West Kunlun	RGI30-13.38232	Surging during 2000 to 2014 (ongoing), peak velocities >250m/yr, terminus advance >1km from 2010 to 2014 with heavy surface crevassing
N2	RGI30-13.38152	Surging during 2000 to 2014 (ongoing), peak velocities > 400m/yr, terminus advance >1km from 2009 to 2014 with heavy surface crevassing
West Yulong	RGI30-13.38255	Probably surging before 1972, terminus slightly advanced in early 1970's, stagnant flow, heavy surface crevassing
Kunlun	RGI30-13.38303	Terminus slightly advanced in early 1970's, stagnant flow (western branch), looped moraines
N7	RGI30-13.38175	Surging during 2000 and 2013 (on going), peak velocities ~200m/yr terminus advance ~2km from 2000 to 2013
Yulong	RGI30-13.38245	Surging between 1977 and 1989, terminus advanced ~2km with heavy surface crevassing, stagnant flow
Bulakebashi	RGI30-13.38211	Surging began ~1977 and lasted ~2000, a bulge formed in 1970's was propagated to down-glacier and reached the terminus by 2000, stagnant flow, heavy surface crevassing
Yake	RGI30-13.38111	Looped moraines, heavy surface crevassing
Southern slope		
Gongxing	RGI30-13.38266	Stagnant flow, heavy surface crevassing, looped moraines (eastern branch)
Zhongfeng	RGI30-13.38172	Surging during 2000 and 2007 (western branch), peak velocities >1000m/yr, terminus advanced ~ 2km from July 2003 to 2005
Chongce	RGI30-13.38216	Surging in 1990s, peak velocities ~800m/yr, terminus advanced ~2km from 1991 to 1998 with heavy surface crevassing

RGIID: glacier ID from randlph glacier inventory.

3.4.1 Velocity development in active phase

Initiation of surging at Chongce glacier

Chongce glacier surged during 1989 - 1998, and surface features and velocity maps suggested that glacier surge initiated from up-glacier to its terminus. Ice mass in reservoir area gradually moved to down-glacier from 1989 to 1991, pushing old crevasses in receiving area. Its terminus advance started between 1992 and 1996. Figure 3.4 and figure 3.5 shows velocity changes which reached up to 200 m/yr over mid-glacier by 1992 and increased up to 800 m/yr over mid-down glacier by 1996, and these facts suggested that flow speed also developed from upper stream. By 1998 the surface heavily crevassed and there was no surging behavior.

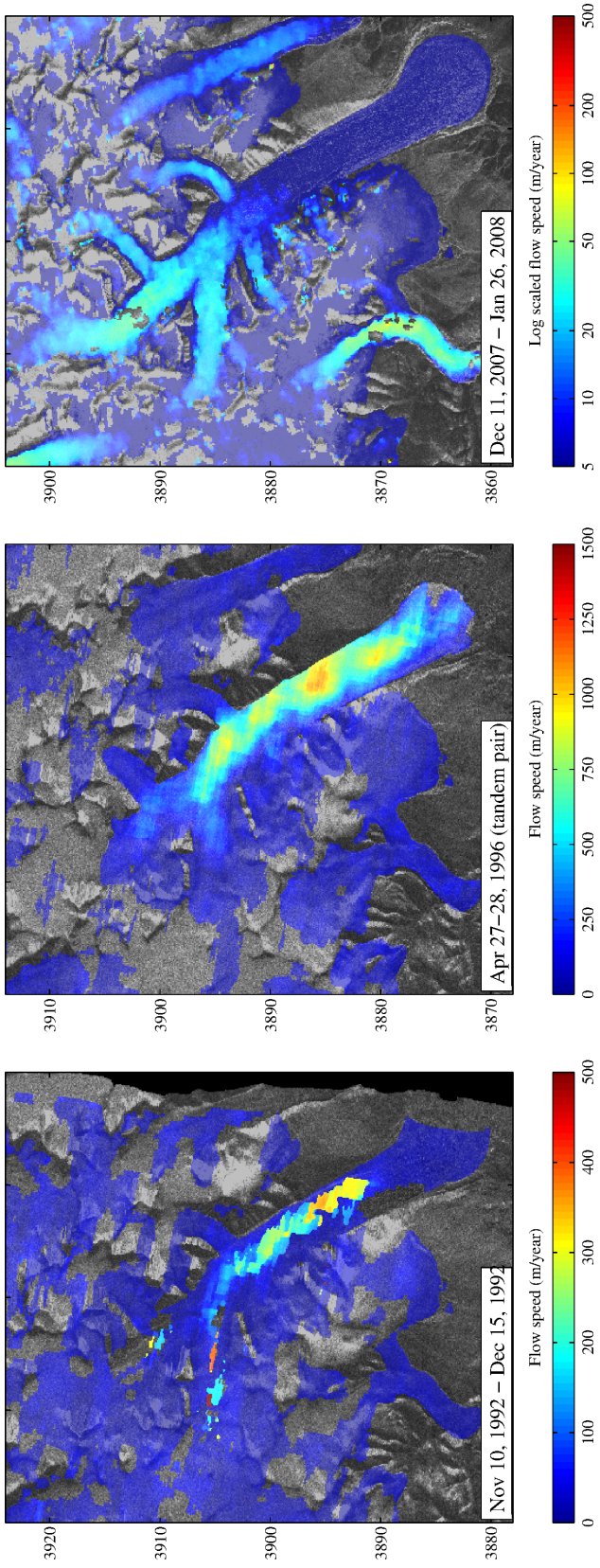

Figure 3.4: Surface velocity maps on Chongce glacier. Early surging stage at 1992, developed stage at 1996 and quiescent velocity at 2007

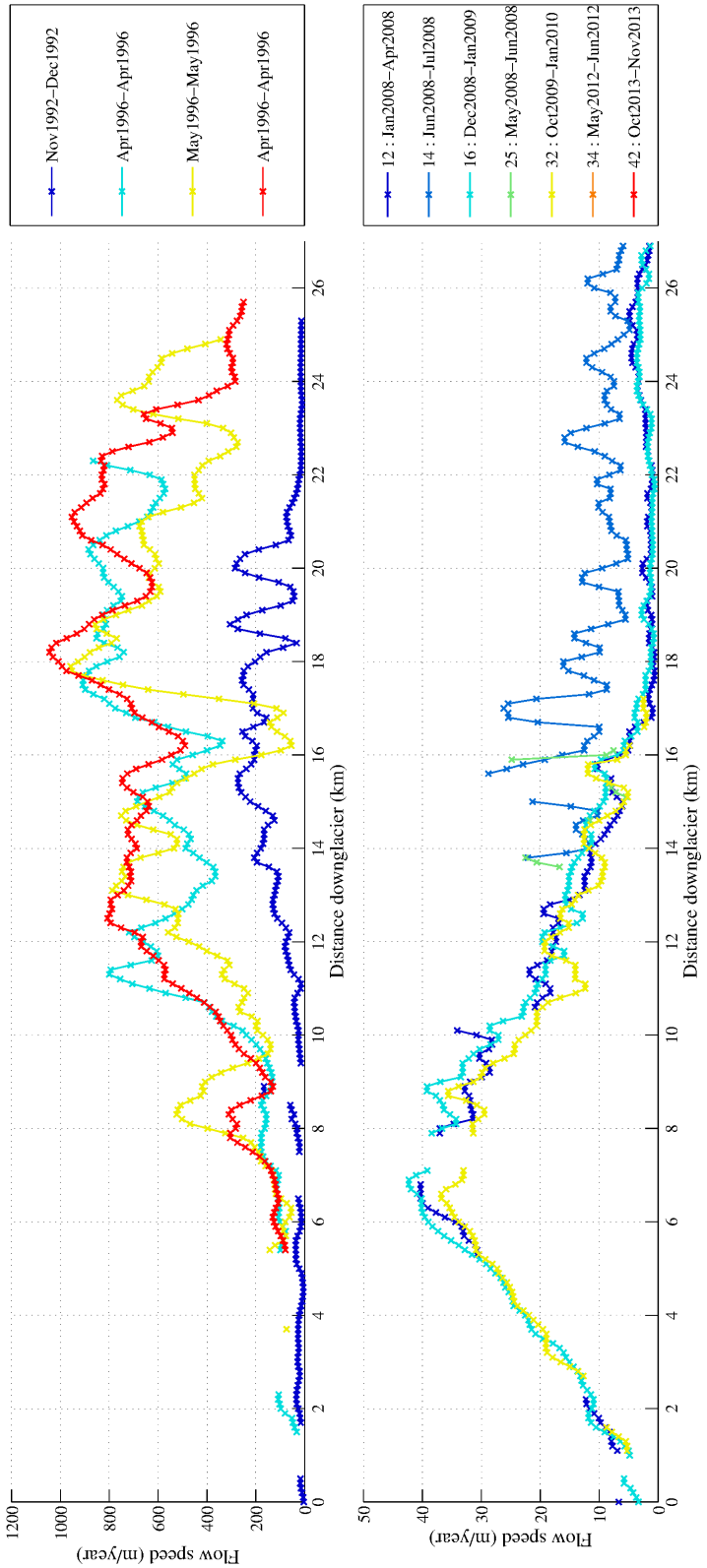

Figure 3.5: Changes in flow speed at Chongce glacier toward down-glacier along flow line

Full surging stage at West Kunlun, N2 and N7 glacier

The initiation of surging at the N2 glacier was uncertain. LSAT images showed that crevasse-free ice in receiving area gradually began to move to down-glacier between 1990 and 1998, reached near the terminus by 2006 and the terminus advanced from Dec 2007 (Fig. 3.9a). Figure 3.6a indicates that the flow speed gradually increased from 100 m/year by 2007 (the blue line in fig 3.6a) to ~250m/year by Feb 2009 (the cyan line in fig 3.6a), and decelerated with advancing from 150m/year by 2013 to 100m/year by 2014 (the yellow and red lines in fig 3.6a).

West Kunlun glacier has three branches whose front positions gradually retreated from 1972, and the eastern branch separated from the others by 2006. The initiation of surging at the West Kunlun Glacier was also uncertain. Expansion of clean-ice area was indicative of first surging signal, which occurred on the eastern branch around 1998 and reached near terminus by 2006, pushing old crevasses on the down-glacier and developing new crevasses along the glacier boundary. The snout swelled gradually and advanced from 2010 (Fig. 3.9a). Figure 3.6b indicates that flow speed gradually accelerated from ~70/year by 2007 (the blue line) to ~150-200m/year by Oct. 2009 - Jun. 2010 (the yellow and orange lines) and decelerated from 300 m/year by 2012 to 250 m/year by Sept 2014 (the red line).

Duration of advancing at N7 glacier was the longest among five surging glaciers. Its snout had been advancing with crevassing toward northeastern direction since 1998, and its direction changed toward north from 2003 along a valley wall. Figure

3.6c shows that flow flow speed gradually increased toward the snout but did not change during 2007 - 2010.

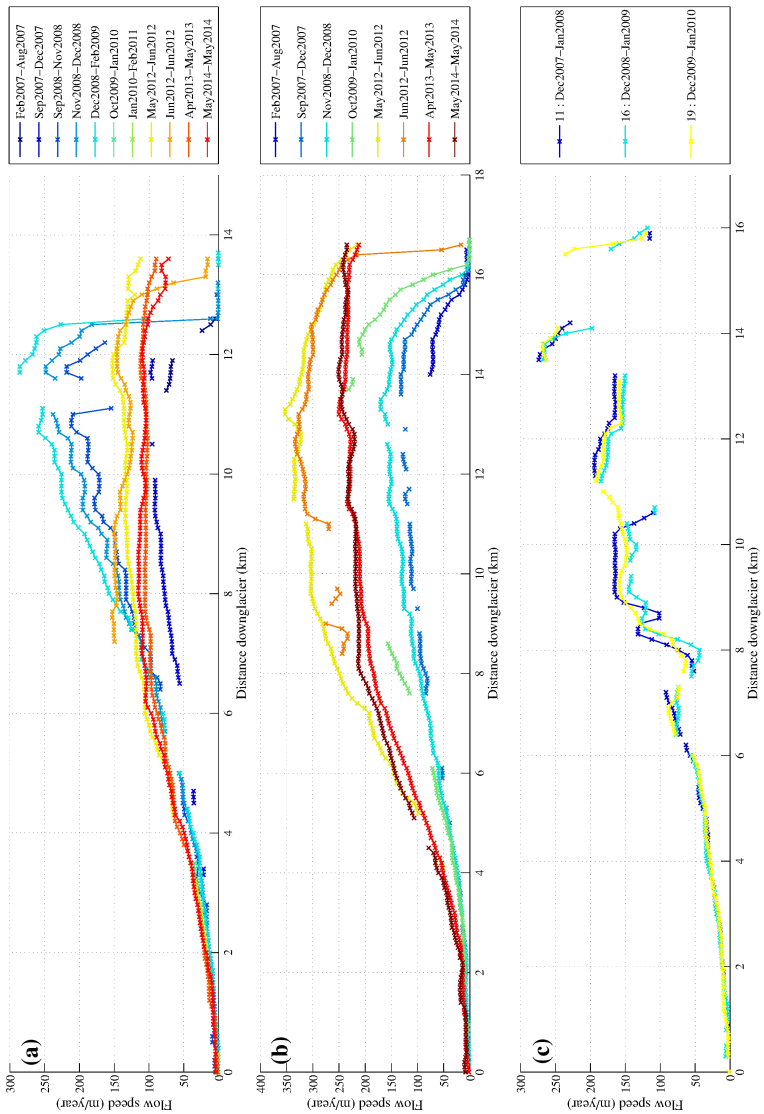

Figure 3.6: Temporal changes in flow speed along down-glacier profile in full surging stage. (a) N2 glacier, (b) West Kunlun glacier, (c) N7 glacier

Termination of surging at Zhongfeng glacier

I detected velocity changes shifted from active phase to quiescent phase and the most rapid advancing in its terminus position at Zhongfeng glacier. The western branch surged around 2000s accompanied with propagation of surge front as extending in crevasse-free area. Its snout abruptly advanced from July 2003 to Nov 2003 and then gradually by Mar 2005 with heavily crevassing. Figure 3.7 shows that surging velocity gradually changed to quiescent velocity during 2004-2007. The flow speed gradually decelerated from 800-1000m/year by 2004 to 40-60m/year by 2007 when glacier flow changed into stagnant flow (Fig. 3.8).

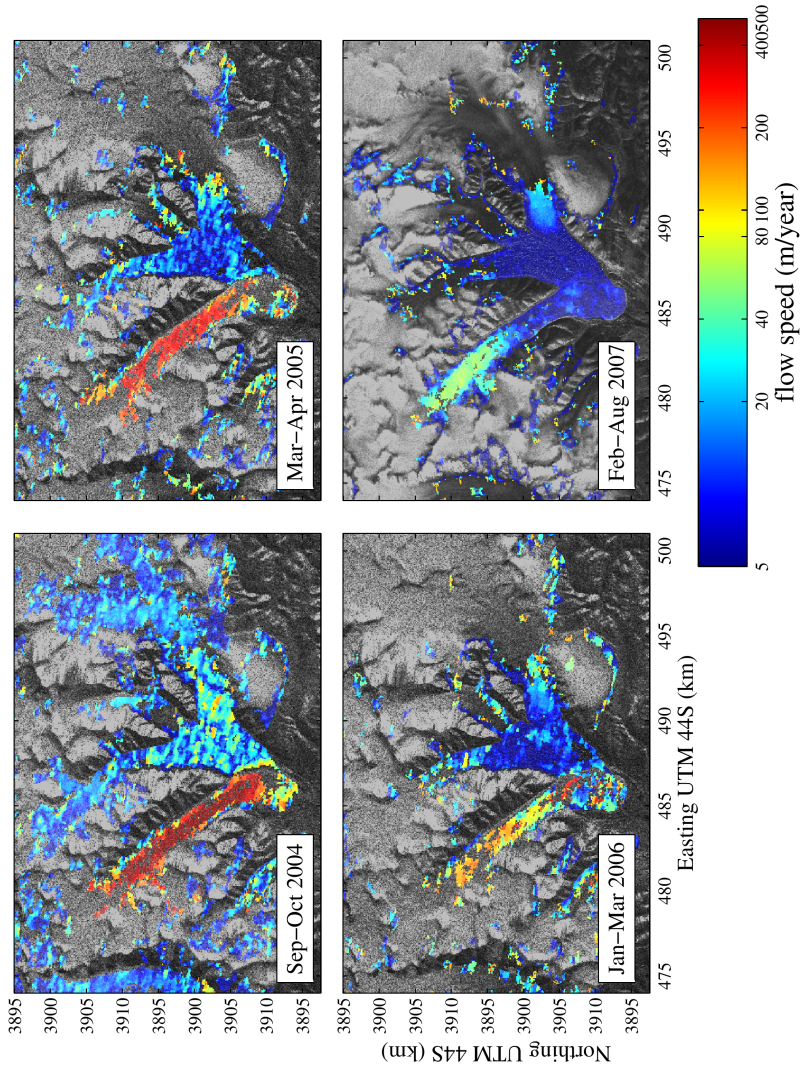

Figure 3.7: Changes in surface velocity map in termination of surging at Zhongfeng glacier

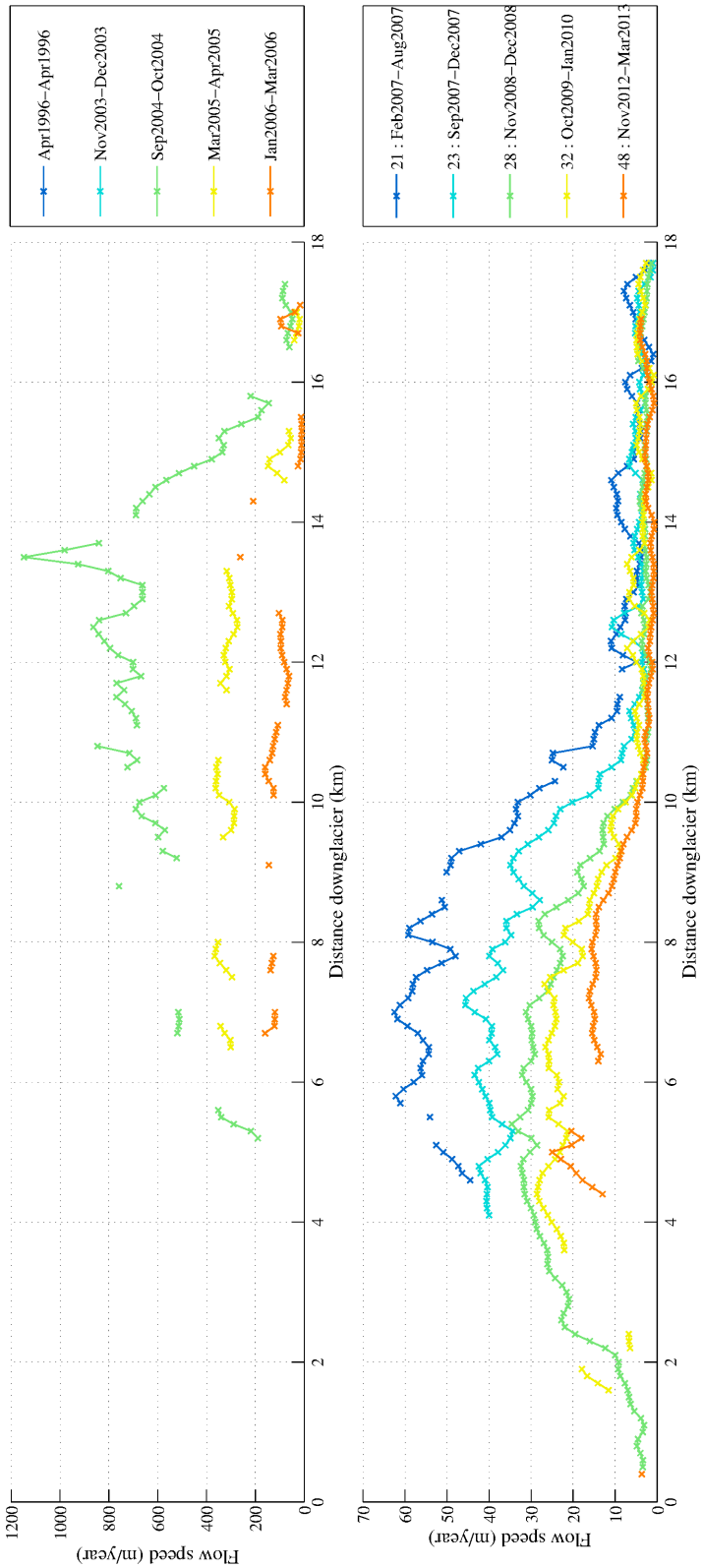

Figure 3.8: Temporal changes in flow speed along down-glacier profile in termination of surging

3.4.2 Changes in glacier terminus position

Changes in glacier terminus position of each category are shown in Figure 3.9. Surge-type glaciers reveal retreat and advance associated with the surge-cycle (Fig. 3.9a). Any surge-type glaciers did not repeat the active phase 1972-2014, which means that surge cycle in WKS was at least 42 years. Nine of the surge-type glaciers advanced but its timing and advancing rate was different each glacier, especially on northern slope or southern slope. For instance, the West Kunlun glacier on the northern slope has three branches of which front position gradually retreated from 1972. The western branches separated from the eastern one and retreated ~2.5 km by 2013. The eastern branch advanced ~1.0 km at a rate of ~130−460 m/yr from 2009 to 2013. The N7 glacier most gradually advanced 2.0 km from 2000 to 2014 at a rate ~120 m/yr. Zhongfeng glacier on the southern slope most rapidly advanced at a rate ~6.3 km/year during July - Nov. 2003, and gradually ~510 m/yr during Nov. 2003 and Mar 2005. When advancing stopped, the total advance reached 2.5 km.

Glacier terminus position at uncertain glaciers ranged -2 km to 0.5 km (Fig. 3.9b). Duota glacier slightly advanced by 1992 and retreated by 2013, probably due to the interaction to proglacial lake. N5 glacier retreated 0.5 km by 1992 then slightly advanced. Duofeng glacier and N4 glacier were merged in 1970 and their snout rapidly shrunk. Duofeng glacier had been retreating up to 2 km by 2014, while terminus retreat at N4 terminated by 2005.

Normal glaciers were almost static compared with the other categories and changes

in their terminus position ranged between ±100m, except for S4 whose snout gradually advanced 300m by 2000 (Fig. 3.9c).

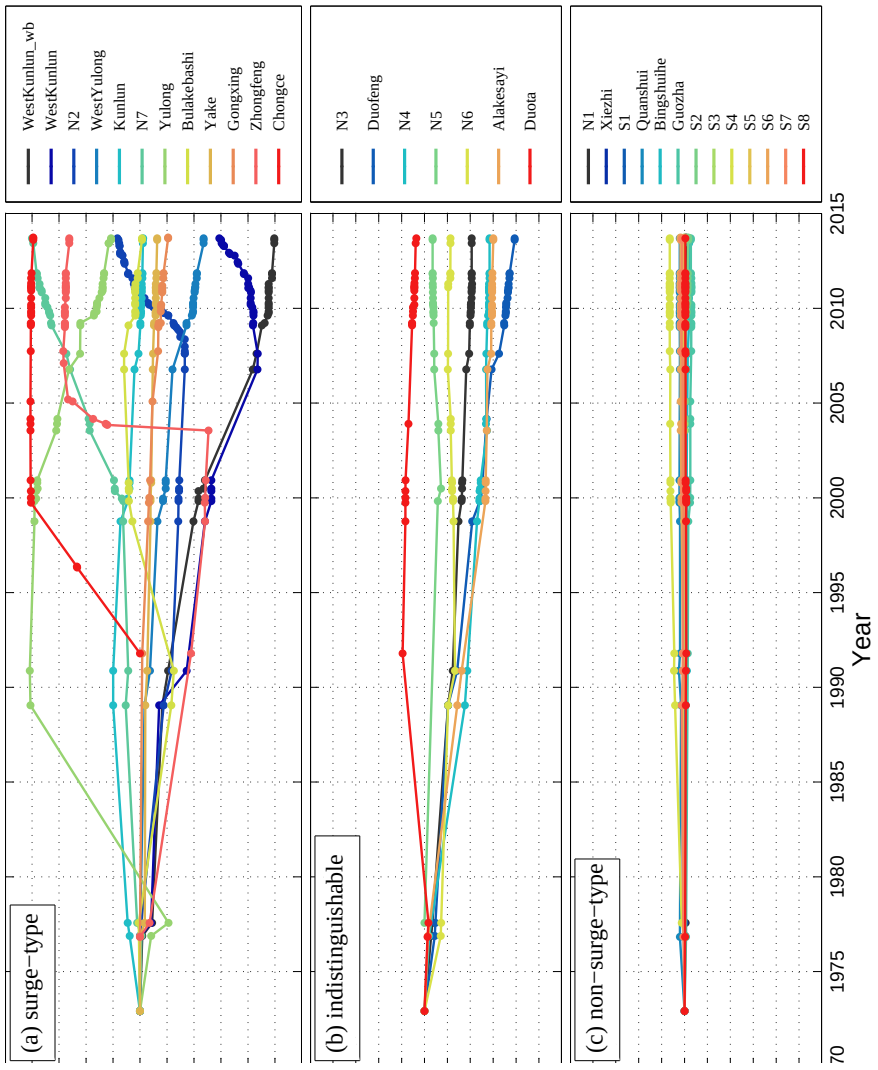

Figure 3.9: Changes in glacier terminus position from 1972 to 2013. (a) surge-type glaciers, including the western branch of West Kunlun glacier, (b) indistinguishable, and (c) non-surge-type (normal) glaciers.

3.4.3 Distribution and characteristics of surge-type glaciers

Distribution of categorized glaciers is shown in Figure 3.4.3. Surge-type glaciers situated on northern and southern slope and relatively large glaciers were categorized. Indistinguishable glaciers located on northern slope, except for Duota glacier. Normal glaciers were relatively small in glacier size and mainly located on the southern slope.

Variations in glacier terminus position were larger on the northern slope than on the southern slope. Since WKS is located on the periphery of Tibetan plateau, mountain shapes are different from each other. On the southern slope whose elevation gradually reduces toward the typical shape of a plateau surface. Piedmont glaciers are dominated and no glaciers develop below 5200 m [Zhang and Jiao, 1987]. On the northern slope where relatively long-steep glaciers flow into the deep incised valley, some glaciers develop below 5000m [Zhang et al., 1989]. Advanced snout on the northern slope depleted rapidly due to the increase in ablation and glaciers might be retreated near dynamic balance line. When ice masses refilled for next surge, so surge advance seemingly became gradual. Meanwhile depletion on the southern slope must be small, retreating was gradual compared with the northern one and remnant ice might exist until next surge. Once glacier surge initiated, a surge front gradually propagated down-glacier pushing remnant ice body, and when it reached the terminus the snout spread rapidly onto the flat plate surface without friction from valley wall. Recalling that surge cycle was at least longer than 42 years and 5 uncertain glaciers

situated on the northern slope, their rapid retreat in the terminus position probably resulted from the past surge advancing [Yde and Knudsen, 2007], but further studies were necessary.

Glacier surge initiated from mid-glacier to down-glacier accompanied with increase in glacier flow but a surge bulge did not appear except for Bulakebashi glacier. When activation of surging reached the terminus, the snout advanced. Surging terminated gradually over several years, concomitant with shifting from surging velocity to quiescent velocity which decreased to 0-20 m/yr. Years-long deceleration/acceleration phase and decades-long quiescent are similar to those in the surge-type glaciers in Svalbard [Fowler et al., 2001, Murray et al., 2003]. However, the finer temporal flow profiles at two surging glaciers indicated that surging glaciers in WKS could be regulated by hydrologically. I will describe the detail results the next session.

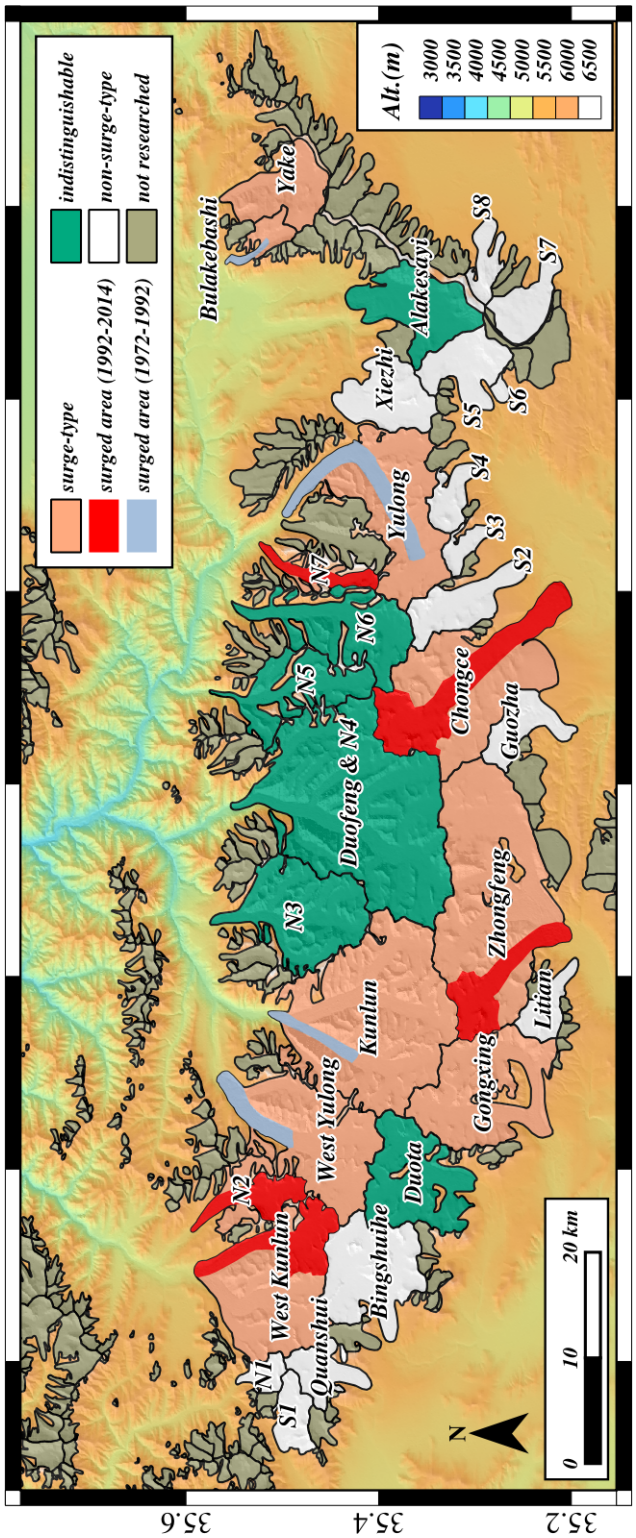

Figure 3.10: Distribution of surge-type glaciers, indistinguishable and normal glaciers. Glacier outlines are RGI v3.2. Each category is filled with colors in upper-right legend. Surging area is filled with different colors before/after 1992.

3.5 Conclusion

I first identified surge-type glaciers in WKS based on several glaciological criteria (Fig. 3.4.3, Table 3.5) [Copland et al., 2003, Grant et al., 2009], using satellite SAR datasets from 1992 and Landsat optical imageries from 1972. Results revealed the distribution and general characteristics of the surge-type glacier in WKS. Of the thirty one major glaciers, 11 glacier were confirmed as surge-type glaciers, 6 glaciers were still suspected as surge-type glaciers and the others were identified as normal type. For surge-type glaciers, flow speed gradually increased up to ~200-1000 m/year in the decade-long active phase and decelerated to ~0-30m/year in the quiescent phase. Since no glacier repeated glacier surging during the analysed period, the surge cycle could be estimated longer than 42 years. These decades-long duration in active and in quiescent phase resembled to the Svalbard-type surges. Variation in the terminus position were different between deeply incised valley shape on the norther slope and flat plate shape on the southern slope. probably due to advance in the glacier snout by past surging caused large depletion on descended ice.

Chapter 4

Glacier Surge Dynamics at the West Kunlun Shan

4.1 Introduction

The rapid flow of surge-type glaciers can be caused by the basal slip including till deformation. The primary factor of the surging is high basal water pressure. When the water pressure exceed a critical value, the basal slip can be destabilize by ice-bed separation and/or weakening of the underlying till. According to the velocity development of surging glacier and the melt water supply, following two possible mechanisms have been proposed.

One is the hydrological regulation mechanism based on the observations of glacier surging at the Variegated Glacier, Alaska [Kamb et al., 1985, Eisen et al., 2005]. The Variegated Glaicer is a temperate land-based soft-bedded glacier. The glacier flow at the Variegated Glacier abruptly switches between quiescent velocity and surging

velocity, initiating in winter and terminating in summer. The duration of surging is typically 1-3 years and quiescent phase is in the order of decades. It seems that the development of surging is coincided with changes in hydraulic systems. Large amounts of meltwater from the surface in summer can be stored englacially, which can gradually move to the glacier sole in winter [Lingle and Fatland, 2003]. Also after melting season, a linked-cavity system can be dominated [Kamb, 1987], in which the drainage is inefficient and the water pressure can be elevated. The elevated water pressure enhanced the basal slip in the winter and could initiate the glacier surging. The surging can be terminated, when an efficient subglacial drainage system was reestablished in summer [Kamb, 1987], decreasing the basal water pressure and strengthening the till layer [Eisen et al., 2005].

On the other hand, the thermal regulated mechanism is proposed based on the observations of surge-type glaciers at Svalbard [Fowler et al., 2001, Murray et al., 2003]. Glaciers at Svalbard are poly-thermal glaciers, overlying sedimentary beds [Murray et al., 2000, Woodward et al., 2003]. Surge-type glaciers at Svalbard generally have years-long surging phase and long quiescent phase which continues decades to over a century. The development of surging gradually initiates and terminates in any season. The peak flow speed of Svalbard surges is generally slower compared to Alaskan surges. Under the sub-polar environment, it seems unlikely to generate amounts of meltwater to trigger the surging. For Svalbard-type surges, it presumes that pressure melting produced amounts of meltwater at the bottom, leading to the initiation of glacier surging. During the glacier surging, friction heat produced fur-

ther meltwater into the bottom of glacier, enhancing the basal slip. The surging flow transports large-ice masses into the down-glacier. The glacier surging terminates when amounts of meltwater could not generate through redistribution of ice.

West Kunlun Shan (WKS) is the one of the driest and the coldest environment around High Mountain Asia. Although an ice cap in WKS is frozen to the bed [Thompson et al., 1995], Aniya [2008] reports that glaciers in WKS are polythermal glaciers. The glacier surface is almost-debris free [Scherler et al., 2011], while the thick basal till often emerges in the downglacier [**?**] and the end moraine exists [Zheng, 1987, **?**]. As mentioned section 3, surge-type glaciers cluster in West Kunlun Shan (WKS). Three glaciers had been surging since early 2000s and the development of glacier flow resembled the Svalbard-type surges. However, the temporal changes of flow speed at two surging glaciers, West Kunlun glacier and the N2 glacier (Fig. 4.1), indicated that hydrological mechanism regulated the surging flow at WKS.

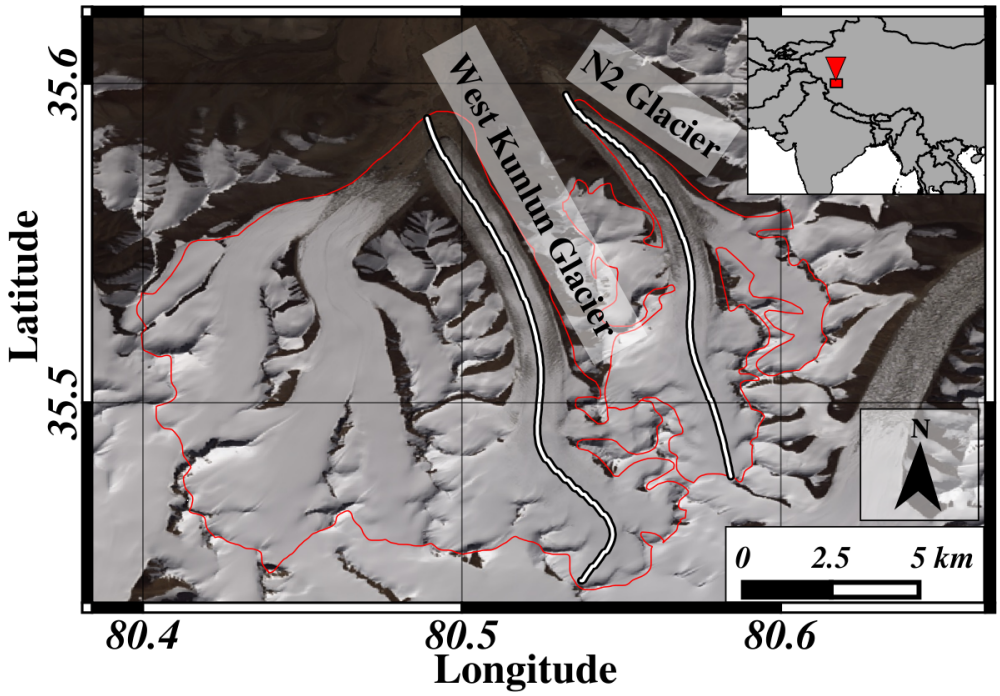

Figure 4.1: Location of the two surging glaciers in the West Kunlun Shan. Thick white lines indicate the flow lines. Background image is Landsat 8 acquired on Sept 27, 2013. The glacier boundry with red lines are based on Randolph Glacier Inventory, version 3.2.

4.2 Seasonal fluctuation in surging flow

Temporal velocity maps derived from ALOS/PALSAR data during 2007 - 2011 and TerraSAR-X data during 2012 - 2014 are shown in figure 4.2. The flow lines set from the glacier terminus (Fig. 4.1). Figure 4.3 and 4.4 show the profile of temporal velocity along the flow line of the N2 and the West Kunlun glacier, respectively. Because of the limited temporal coverages and the failure of processing data, it is uncertain when the glacier flow accelerated at both glaciers. Although the flow speed gradually decelerated by 2014, both glaciers were still surging, indicating that the duration of the active phase is longer than 7 years.

At the N2 glacier in Figure 4.3, the flow speed gradually accelerated from ~100 m/yr by 2007 to ~250 m/yr by Feb 2009. The terminus had been advancing since Feb 2009. The flow speed gradually decelerated from 2013. In the deceleration phase, the flow velocities modulated seasonally. The velocities slowed down in April to June and speeded up in Oct-Jan. The peak velocities in fall-winter reached to 220 m/yr in 2012 and 180 m/yr in 2013. The amplitude of seasonal velocity in 2013 reached up to 170% (Fig. 4.5).

At the West Kunlun Glacier in Figure 4.4, the flow speed fluctuated seasonally through in the acceleration phase and the deceleration phase. The winter velocities reached up-to 130 m/yr in 2007, 200 m/yr in 2008, 220 m/yr in 2009, 500 m/yr in 2012 and 440 m/yr in 2013. The summer velocities were slower than the winter one, and reached up-to 80-100 m/yr in 2008, 130 m/yr in 2009, 330 m/yr in 2012, 240

m/yr in 2013 and 250 m/yr in 2014. The amplitude of seasonal velocity reached up to nearly 200% (Fig. 4.5).

The thermal regulation mechanism is based on surging episode at the Monacobreen, Svalbard during 1990s [Murray et al., 2003]. The velocity developments were derived from ERS 1/2 tandem and ice-phase InSAR mission with the 1 day and 3 days recurrent period, which were mainly during winter periods. Sund et al. [2014] observed higher velocities of surging in summer than in winter at the Nathorstbreen glacier system, Svalbard, during 2010-2012. They suggested that large amounts of meltwater from the surface and the bottom were able to trap into englacial water storages during the active phase, which influenced the basal motion under polythermal glaciers.

Surface velocity observations at other glaciers in WKS indicate a variety of seasonal changes [Yasuda and Furuya, 2013]. The glaciers in WKS are a summer accumulation-type and accumulation and ablation mainly occur during a summer period (May-Aug) [Zhang and Jiao, 1987]. The well-known summer speed-up and winter slow-down appeared at Duofeng Glacier, the largest valley glacier on the norther slope in WKS. It is unlikely that surface meltwater production is spatially heterogeneous over the studied WKS area. Therefore, the meltwater storage and discharge processes will be different at each glacier.

The speculated surging processes are as follows. During the active phase, it could expect that an increase of the cavity size on the leeward side of the bumpy bed, generating more and more interconnected cavities [Iken and Truffer, 1997]. Surface

meltwater were delivered into the bed through the side valley and/or the crevasse opening. The summer meltwater cannot drain efficiently and a portion of the meltwater will remain until late fall to winter. During the absence of surface meltwater input, creep closure will reduce the total volume of isolated cavities, enchanting the water pressure and overlying ice speed. The flow speed slowed down when isolated cavities connected to the main drainage, reducing the water pressure. As long as there are enough ice mass in the reservoir are, glacier surging could continue and the seasonal cycle may repeat.

It remains uncertain how surface meltwater influenced on the initiation and the termination of polythermal glacier surges. Also the pressure melting and frictional heating processes can generate the water at the ice bottom, which may assist to initiate and evolve the surging. The two surging were still on going and further studies were necessary to solve the whole processing of glacier surging in WKS.

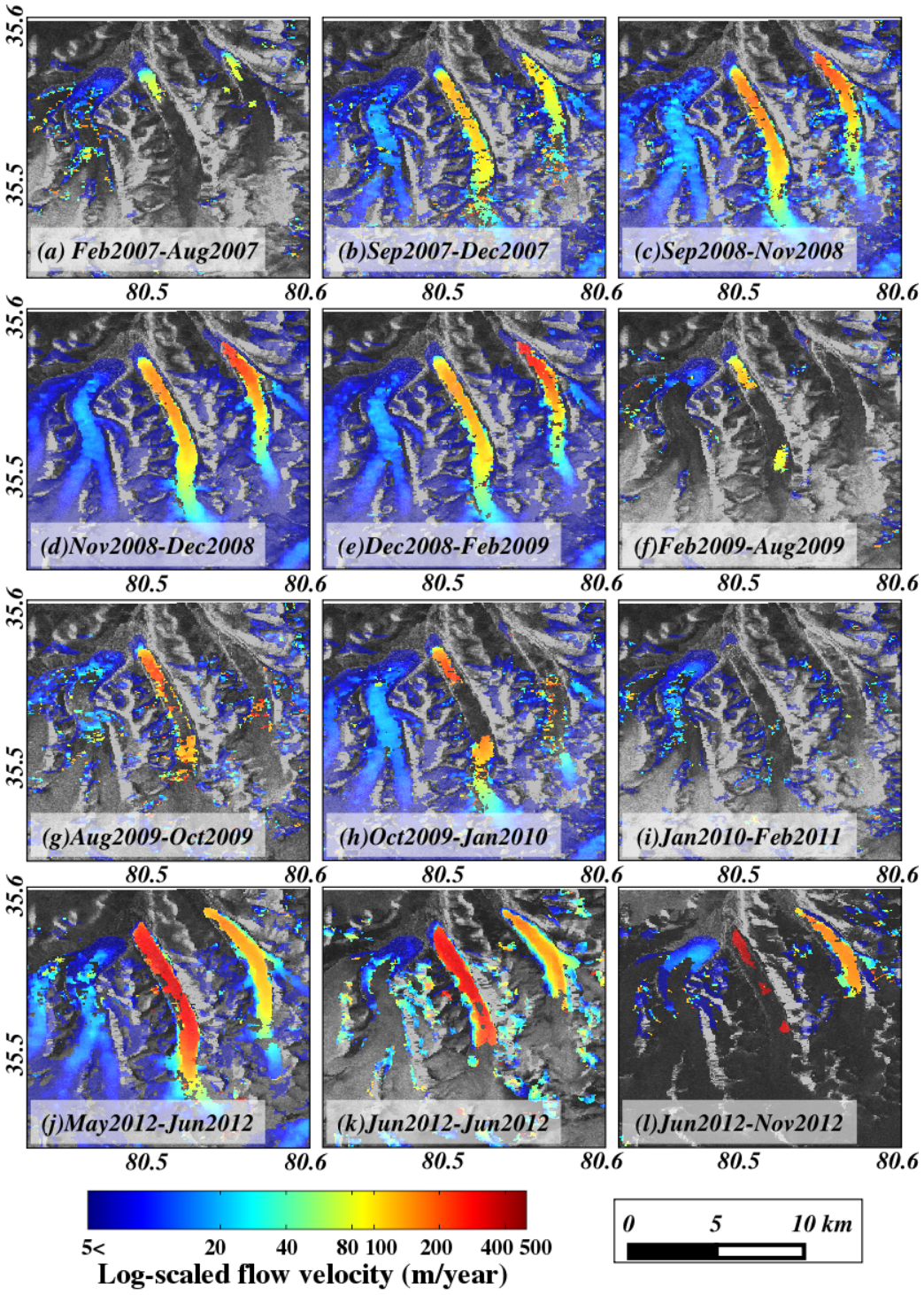

Figure 4.2: Temporal velocity maps at West Kunlun glacier and N2 glacier from 2007 to 2014.

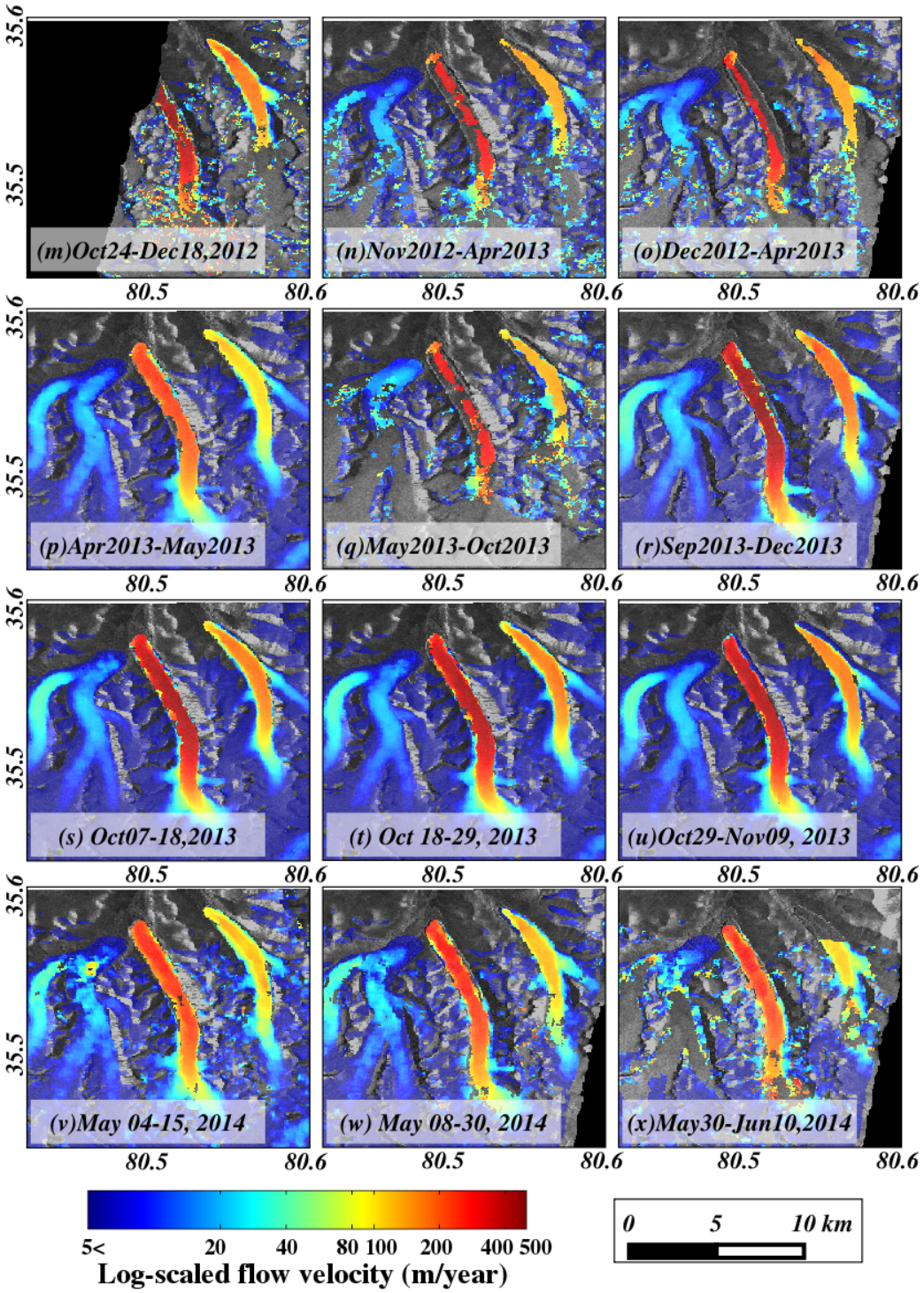

Figure 4.2: (continued)

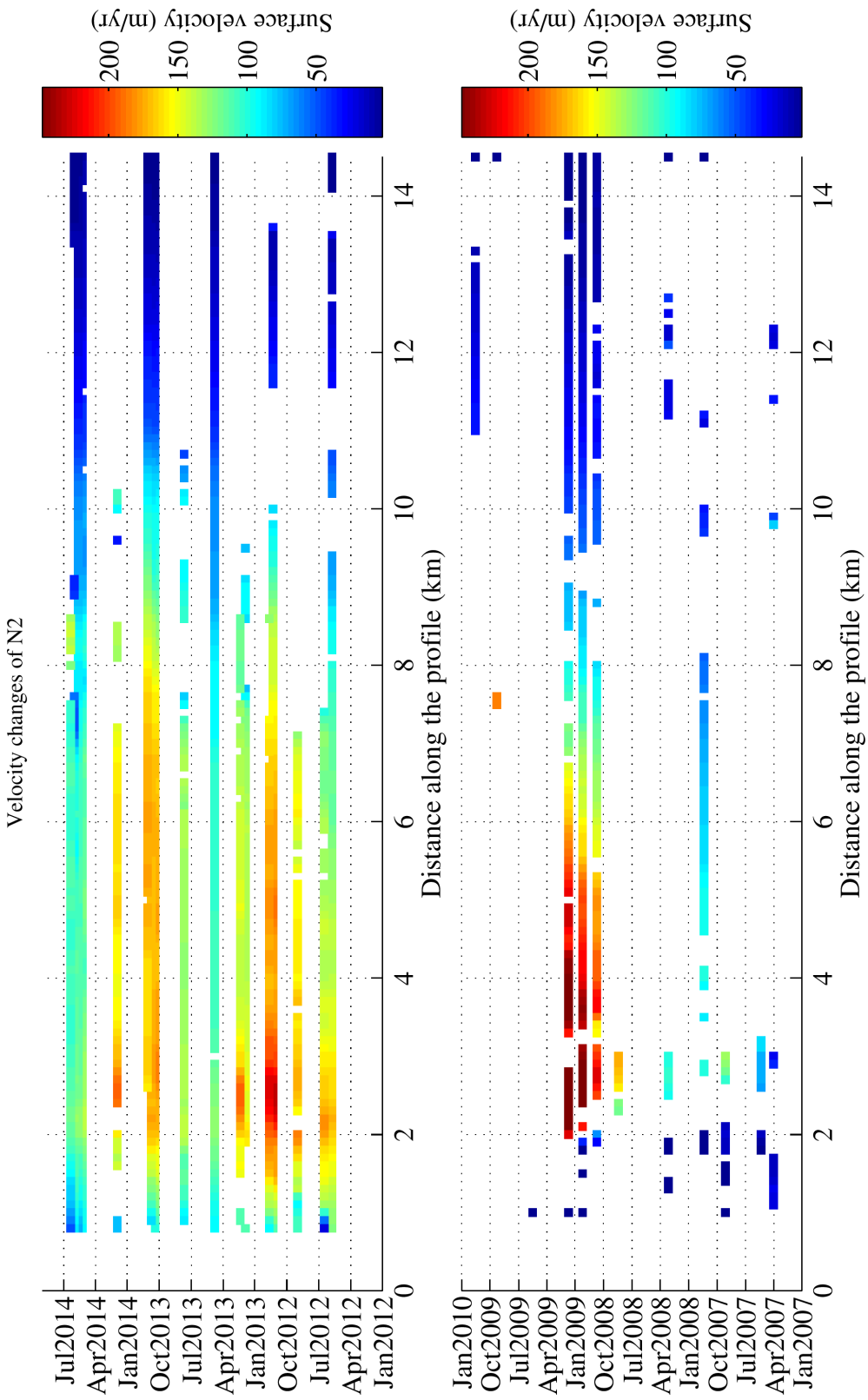

Figure 4.3: Temporal flow speed at N2 glacier along flow line to down-glacier

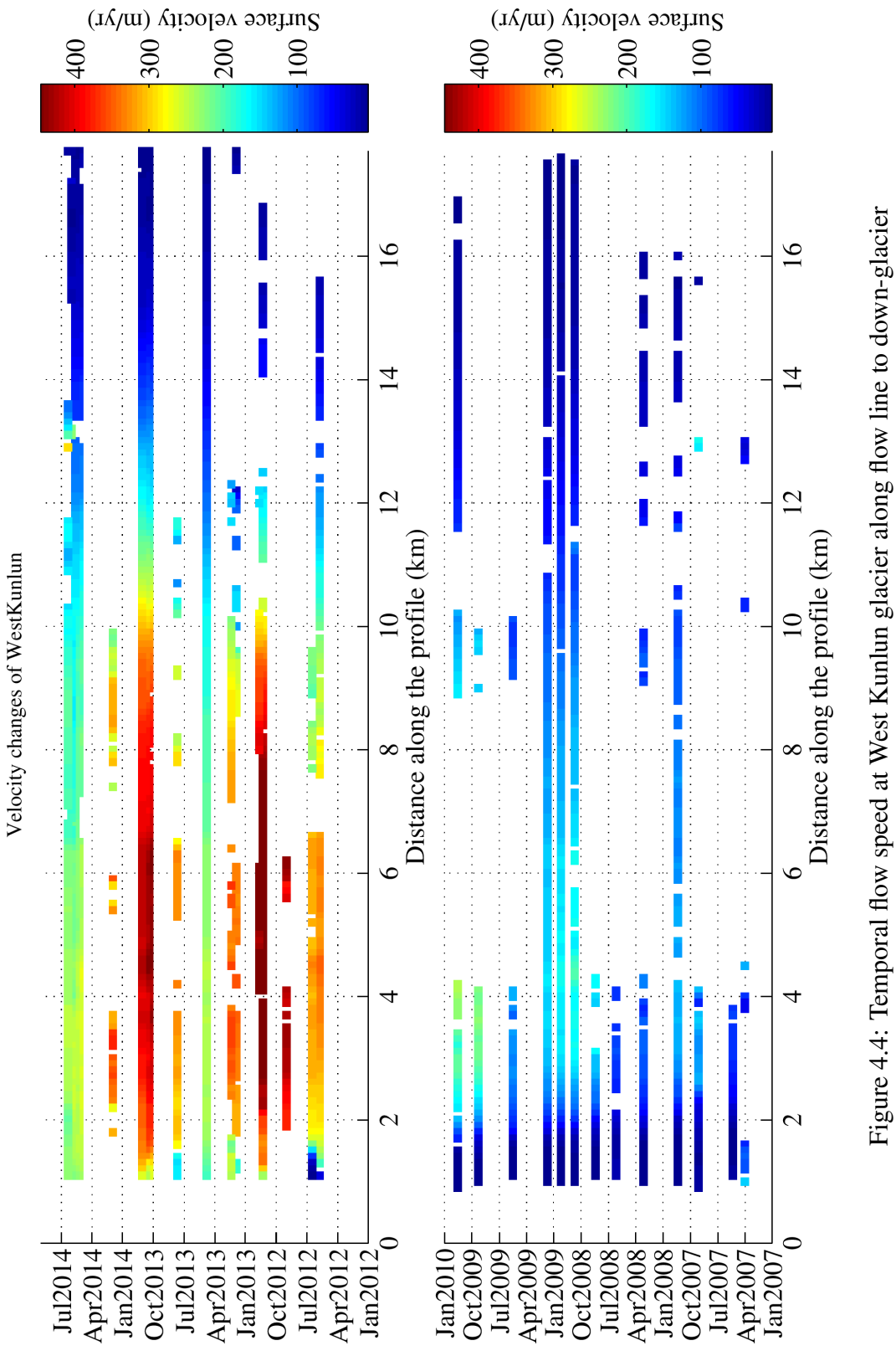

Figure 4.4: Temporal flow speed at West Kunlun glacier along flow line to down-glacier

4.3 Conclusion

I focused on two surging glaciers in WKS and their flow dynamics using different satellite SAR datasets from 2003 to 2014, up to 46 days and 11 days temporal resolution with ALOS/PALSAR imageries from 2007 to 2011 and TerraSAR-X imageries from 2012, respectively. Results reveals that surging flow accelerated and decelerated over seven years accompanied with seasonal fluctuation. The surging flow speeded up during fall to winter and slowed down in summer. The amplitude of peak velocity reached up to 180-200% in 2013. This indicated that surface meltwater could be delivered into the bottom of polythermal glaciers during surging, influencing the basal slip though the englacial water storages and discharge processing.

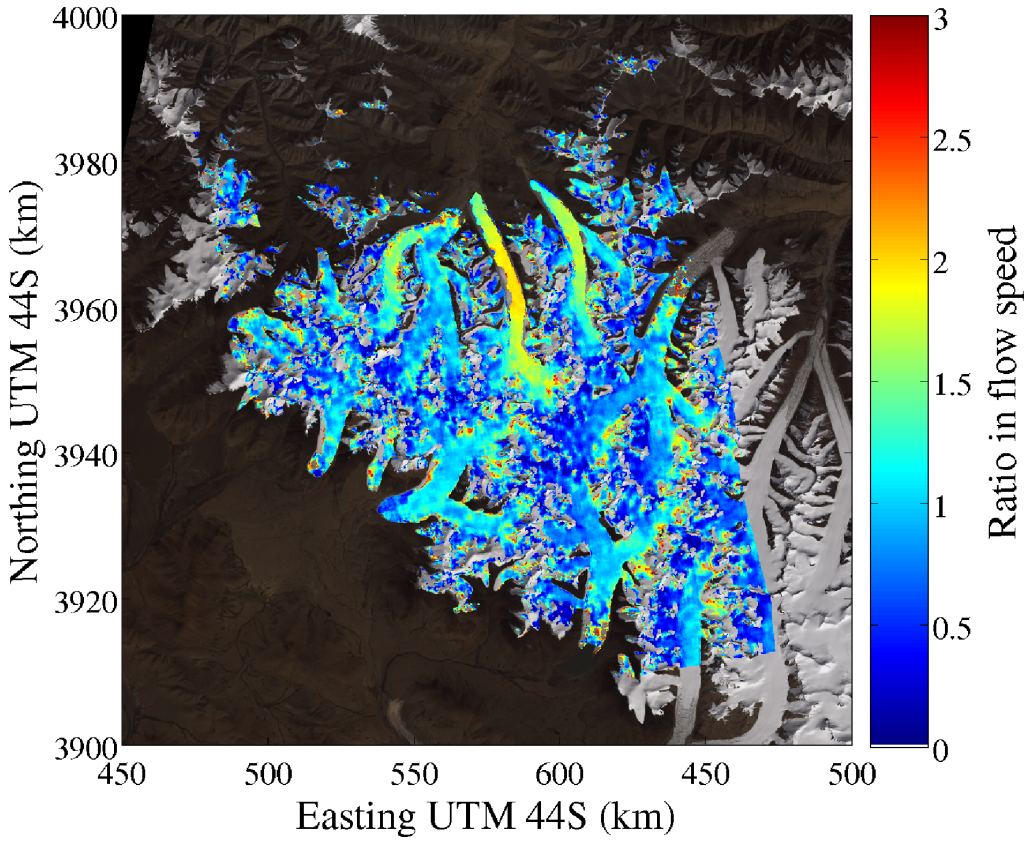

Figure 4.5: Ratio of increase in surface velocity during Oct. 10-18, 2013 against Apr. - May, 2013.

Chapter 5

Conclusion

Unnoticed surge-type glaciers in West Kunlun Shan, located in northwestern Tibetan plateau, were caused uncertainty in assessment of climate change through reduction in glacier area and its thickness. Using satellite remote sensing from 1972 to 2014, I first clarified distribution and general characteristics of surge-type glacier this region. Furthermore, temporal velocity maps were revealed surging flow seasonally fluctuated result from influx of meltwater from the surface that were not considered for Svalbard mechanism where ice thickness and thermal regime are responsible for surge progress. The major results I conducted are summarized as follow:

Chapter 3: “ Surge-type glaciers in West Kunlun Shan ”

(1) Surge-type glaciers were identified based on surface velocity maps, changes in

terminus position and visible surface features, using four different SAR datasets and Landsat optical imageries.

(2) Of thirty one major glacier in WKS, 11 glaciers were confirmed as surge-type and 5 were suspected. Year-long surging flow gradually accelerated up to ~200-1000m/year and decelerated ~0-30m/year, following quiescent phase continued at least 42 years.

(3) Reduction in glacier area on the northern slope were probably result from increase in ablation due to past surging.

Chapter 4: " Glacier surge dynamics at the West Kunlun Shan "

(1) Two surging glacier were detected with ALOS/PALSAR (46-day repeat) and TerraSAR-X (11-day repeat) imageries and its flow speed increased up to 180-200% in October against Apr-May, 2013.

(2) Years-long acceleration and deceleration in WKS were resembled to the Svalbard-type surges. The seasonal fluctuation, however, indicated that surging glaciers in WKS were also regulated by the hydrological processing, in which meltwater input from the surface preceded summer could play an important role.

Bibliography

M. Aniya. Landforms and Glaciers of the Western Kunlun Mountains, China (Japanese). *Himalayan Study Monographs*, 9:192–208, 2008.

T. Bolch, A. Kulkarni, A. Kääb, C. Huggel, F. Paul, J. G. Cogley, H. Frey, J. S. Kargel, K. Fujita, M. Scheel, S. Bajracharya, and M. Stoffel. The state and fate of Himalayan glaciers. *Science*, 336(6079):310–4, Apr. 2012. ISSN 1095-9203. doi: 10.1126/science.1215828.

L. Copland, T. Sylvestre, M. P. Bishop, J. F. Shroder, Y. B. Seong, L. a. Owen, A. Bush, and U. Kamp. Expanded and Recently Increased Glacier Surging in the Karakoram. *Arctic, Antarctic, and Alpine Research*, 43(4):503–516, Nov. 2011. ISSN 1523-0430. doi: 10.1657/1938-4246-43.4.503.

L. D. Dolgoushin and G. B. Osipova. Glacier surges and the problem of their forecasting. *IAHS Publ*, 104:292–304, 1975.

O. Eisen, W. D. Harrison, C. F. Raymond, K. a. Echelmeyer, G. a. Bender, and J. L. Gorda. Variegated Glacier, Alaska, USA: a century of surges.

Journal of Glaciology, 51(174):399–406, June 2005. ISSN 00221430. doi: 10.3189/172756505781829250.

A. Fowler, T. Murray, and F. Ng. Thermally controlled glacier surging. *Journal of Glaciology*, 47(159):527–538, Oct. 2001. ISSN 00221430. doi: 10.3189/172756501781831792.

A. S. Gardner, G. Moholdt, J. G. Cogley, B. Wouters, A. a. Arendt, J. Wahr, E. Berthier, R. Hock, W. T. Pfeffer, G. Kaser, S. R. M. Ligtenberg, T. Bolch, M. J. Sharp, J. O. Hagen, M. R. van den Broeke, and F. Paul. A reconciled estimate of glacier contributions to sea level rise: 2003 to 2009. *Science (New York, N.Y.)*, 340 (6134):852–7, May 2013. ISSN 1095-9203. doi: 10.1126/science.1234532.

R. M. Goldstein, H. Engelhardt, B. Kamb, and R. M. Frolich. Satellite radar interferometry for monitoring ice sheet motion: application to an antarctic ice stream. *Science (New York, N.Y.)*, 262(5139):1525–30, Dec. 1993. ISSN 0036-8075. doi: 10.1126/science.262.5139.1525.

A. Gray, K. Mattar, P. Vachon, R. Bindschadler, K. Jezek, R. Forster, and J. Crawford. InSAR results from the RADARSAT Antarctic Mapping Mission data: estimation of glacier motion using a simple registration procedure. In *IGARSS '98. Sensing and Managing the Environment. 1998 IEEE International Geoscience and Remote Sensing. Symposium Proceedings. (Cat. No.98CH36174)*, number 1, pages 1638–1640 vol.3. IEEE, 1998. ISBN 0-7803-4403-0. doi: 10.1109/IGARSS.1998.691662.

W. Guo, S. Liu, J. Wei, and W. Bao. The 2008/09 surge of central Yulinchuan glacier, northern Tibetan Plateau, as monitored by remote sensing. *Annals of Glaciology*, 54(63):299–310, July 2013. ISSN 02603055. doi: 10.3189/2013AoG63A495.

W. D. Harrison and A. S. Post. How much do we really know about glacier surging? *Annals of Glaciology*, 36(1):1–6, Jan. 2003. ISSN 02603055. doi: 10.3189/172756403781816185.

J. P. M. Hendriks and P. P. Helsinki. Semi-automatic glacier delineation from Landsat imagery over Hintereisferner in the Austrian Alps. *Zeitschrift fur Gletscherkunde und Glazialgeologie*, 41:55–75, 2007.

K. Hewitt. Tributary glacier surges: an exceptional concentration at Panmah Glacier, Karakoram Himalaya. *Journal of Glaciology*, 53(181):181–188, Mar. 2007. ISSN 00221430. doi: 10.3189/172756507782202829.

A. Iken and M. Truffer. The relationship between subglacial water pressure and velocity of Findelengletscher, Switzerland, during its advance and retreat. *Journal of Glaciology*, 43(1), 1997.

A. Jarvis, H. Reuter, A. Nelson, and E. Guevara. Hole-filled SRTM for the globe Version 4, available from the CGIAR-CSI SRTM 90m Database (http://srtm.csi.cgiar.org), 2008.

H. Jiskoot. *Encyclopedia of Snow, Ice and Glaciers: Glacier Surging (p415-428)*. Springer, 2011. ISBN 978-90-481-2641-5.

H. Jiskoot, T. Murray, and P. Boyle. Controls on the distribution of surge-type glaciers in Svalbard. *Journal of Glaciology*, 46(154):412–422, Aug. 2000. ISSN 00221430. doi: 10.3189/172756500781833115.

I. Joughin, R. Kwok, and M. Fahnestock. Estimation of ice-sheet motion using satellite radar interferometry: method and error analysis with application to Humboldt Glacier, Greenland. *Journal of Glaciology*, 42(142):564–575, 1996.

I. Joughin, R. Kwok, and M. Fahnestock. Interferometric estimation of three-dimensional ice-flow using ascending and descending passes. *IEEE Transactions on Geoscience and Remote Sensing*, 36(1):25–37, 1998. ISSN 01962892. doi: 10.1109/36.655315.

I. Joughin, B. E. Smith, and W. Abdalati. Glaciological advances made with interferometric synthetic aperture radar. *Journal of Glaciology*, 56(200):1026–1042, Dec. 2010. ISSN 00221430. doi: 10.3189/002214311796406158.

I. R. Joughin, D. P. Winebrenner, and M. A. Fahnestock. Observations of ice-sheet motion in Greenland using satellite radar interferometry. *Geophysical Research Letters*, 22(5):571–574, Mar. 1995. ISSN 00948276. doi: 10.1029/95GL00264.

B. Kamb. Glacier surge mechanism based on linked cavity configuration of the basal water conduit system. *Journal of Geophysical Research*, 92(B9):9083, 1987. ISSN 0148-0227. doi: 10.1029/JB092iB09p09083.

B. Kamb, C. F. Raymond, W. D. Harrison, H. Engelhardt, K. a. Echelmeyer,

N. Humphrey, M. M. Brugman, and T. Pfeffer. Glacier surge mechanism: 1982-1983 surge of variegated glacier, alaska. *Science*, 227(4686):469–79, Feb. 1985. ISSN 0036-8075. doi: 10.1126/science.227.4686.469.

C. Lingle and D. Fatland. Does englacial water storage drive temperate glacier surges ? *Annals of Glaciology*, 36, 2003. doi: http://dx.doi.org/10.3189/172756403781816464.

Q. Ma, B. Zheng, K. Jiao, I. Shuji, and H. Fushimi. Glacial geomorphological features in upper reaches of the Yurunkar River on the north slope of the West Kunlun Mountains. *Bulletin of glacier research*, 7:139–144, 1989.

K. Mattar, P. Vachon, D. Geudtner, A. Gray, I. Cumming, and M. Brugman. Validation of alpine glacier velocity measurements using ERS Tandem-Mission SAR data. *IEEE Transactions on Geoscience and Remote Sensing*, 36(3):974–984, May 1998. ISSN 01962892. doi: 10.1109/36.673688.

F. Maussion, D. Scherer, T. Mölg, E. Collier, J. Curio, and R. Finkelnburg. Precipitation Seasonality and Variability over the Tibetan Plateau as Resolved by the High Asia Reanalysis*. *Journal of Climate*, 27(5):1910–1927, Mar. 2014. ISSN 0894-8755. doi: 10.1175/JCLI-D-13-00282.1.

R. W. McNabb and R. Hock. Alaska tidewater glacier terminus positions, 1948-2012. *Journal of Geophysical Research: Earth Surface*, 119(2):153–167, Feb. 2014. ISSN 21699003. doi: 10.1002/2013JF002915.

M. Meier and A. Post. What are glacier surges? *Canadian Journal of Earth Sciences*, 6:807–817, 1969.

M. F. Meier, M. B. Dyurgerov, U. K. Rick, S. O'neel, W. T. Pfeffer, R. S. Anderson, S. P. Anderson, and A. F. Glazovsky. Glaciers dominate eustatic sea-level rise in the 21st century. *Science*, 317(5841):1064–7, Aug. 2007. ISSN 1095-9203. doi: 10.1126/science.1143906.

J. Mohr, N. Reeh, and S. Madsen. Three-dimensional glacial flow and surface elevation measured with radar interferometry. *Nature*, 1984:273–276, 1998. doi: 10.1038/34635.

T. Moon and I. Joughin. Changes in ice front position on Greenland's outlet glaciers from 1992 to 2007. *Journal of Geophysical Research*, 113(F2):F02022, June 2008. ISSN 0148-0227. doi: 10.1029/2007JF000927.

T. Murray, G. W. Stuart, P. J. Miller, J. Woodward, A. M. Smith, P. R. Porter, and H. Jiskoot. Glacier surge propagation by thermal evolution at the bed. *Journal of Geophysical Research*, 105(B6):13491, 2000. ISSN 0148-0227. doi: 10.1029/2000JB900066.

T. Murray, T. Strozzi, A. Luckman, H. Jiskoot, and P. Christakos. Is there a single surge mechanism? Contrasts in dynamics between glacier surges in Svalbard and other regions. *Journal of Geophysical Research*, 108(B5):2237, 2003. ISSN 0148-0227. doi: 10.1029/2002JB001906.

T. Nagler, H. Rott, M. Hetzenecker, K. Scharrer, E. Magnusson, D. Floricioiu, and C. Notarnicola. Retrieval of 3D-glacier movement by high resolution X-band SAR data. In *2012 IEEE International Geoscience and Remote Sensing Symposium*, volume 1, pages 3233–3236. IEEE, July 2012. ISBN 978-1-4673-1159-5. doi: 10.1109/IGARSS.2012.6350735.

J. Neelmeijer, M. Motagh, and H.-U. Wetzel. Estimating Spatial and Temporal Variability in Surface Kinematics of the Inylchek Glacier, Central Asia, using TerraSAR—X Data. *Remote Sensing*, 6(10):9239–9259, Sept. 2014. ISSN 2072-4292. doi: 10.3390/rs6109239.

W. T. Pfeffer, A. a. Arendt, A. Bliss, T. Bolch, J. G. Cogley, A. S. Gardner, J.-O. Hagen, R. Hock, G. Kaser, C. Kienholz, E. S. Miles, G. Moholdt, N. Mölg, F. Paul, V. Radic, P. Rastner, B. H. Raup, J. Rich, and M. J. Sharp. The Randolph Glacier Inventory: a globally complete inventory of glaciers. *Journal of Glaciology*, 60(221):537–552, 2014. ISSN 00221430. doi: 10.3189/2014JoG13J176. URL `http://www.igsoc.org/journal/60/221/j13J176.html`.

D. J. Quincey, M. Braun, N. F. Glasser, M. P. Bishop, K. Hewitt, and A. Luckman. Karakoram glacier surge dynamics. *Geophysical Research Letters*, 38(18): L18504, Sept. 2011. ISSN 0094-8276. doi: 10.1029/2011GL049004.

M. Rankl, C. Kienholz, and M. Braun. Glacier changes in the Karakoram region mapped by multimission satellite imagery. *The Cryosphere*, 8(3):977–989, May 2014. ISSN 1994-0424. doi: 10.5194/tc-8-977-2014.

C. F. Raymond. How do glaciers surge? A review. *Journal of Geophysical Research*, 92(B9):9121, 1987. ISSN 0148-0227. doi: 10.1029/JB092iB09p09121.

E. Rignot, K. C. Jezek, and H. G. Sohn. Ice flow dynamics of the Greenland Ice Sheet from SAR interferometry. *Geophysical Research Letters*, 22(5):575–578, Mar. 1995. ISSN 00948276. doi: 10.1029/94GL03381.

E. Rignot, R. Forster, and B. Isacks. Interferometric radar observations of Glacier San Rafael, Chile. *Journal of Glaciology*, 4(42(141)):279–291, 1996.

E. J. Rignot. North and Northeast Greenland Ice Discharge from Satellite Radar Interferometry. *Science*, 276(5314):934–937, May 1997. ISSN 00368075. doi: 10.1126/science.276.5314.934.

H. Rott, M. Stuefer, A. Siegel, P. Skvarca, and A. Eckstaller. Mass fluxes and dynamics of Moreno Glacier, Southern Patagonia Icefield. *Geophysical Research Letters*, 25(9):1407–1410, May 1998. ISSN 00948276. doi: 10.1029/98GL00833.

D. Scherler, B. Bookhagen, and M. R. Strecker. Spatially variable response of Himalayan glaciers to climate change affected by debris cover. *Nature Geoscience*, 4(3):156–159, Jan. 2011. ISSN 1752-0894. doi: 10.1038/ngeo1068.

D. Shangguan, S. Liu, Y. DIng, J. Li, Y. Zhang, L. Ding, X. Wang, C. Xie, and G. Li. Glacier changes in the west Kunlun Shan from 1970 to 2001 derived from Landsat TM/ETM+ and Chinese glacier inventory data. *Annals of Glaciology*, 46 (1):204–208, Oct. 2007. ISSN 02603055. doi: 10.3189/172756407782871693.

T. Strozzi, A. Luckman, T. Murray, U. Wegmuller, and C. Werner. Glacier motion estimation using SAR offset-tracking procedures. *IEEE Transactions on Geoscience and Remote Sensing*, 40(11):2384–2391, Nov. 2002. ISSN 0196-2892. doi: 10.1109/TGRS.2002.805079.

M. Sund, T. R. Lauknes, and T. Eiken. Surge dynamics in the Nathorstbreen glacier system, Svalbard. *The Cryosphere*, 8(2):623–638, Apr. 2014. ISSN 1994-0424. doi: 10.5194/tc-8-623-2014.

L. G. Thompson, E. Mosley-Thompson, M. Davis, P. Lin, J. Dai, J. Bolzan, and T. Yao. A 1000 year climatic ice-core record from the Guliya ice cap, China: its relationship to global climate variability. *Annals of Glaciology*, 21:175–181, 1995.

U. Wegmüller and C. Werner. Gamma SAR processor and interferometry software. In *Third ERS Symposium on Space at the service of our Environment*, volume 414, page 1687, 1997.

J. Woodward, T. Murray, R. a. Clark, and G. W. Stuart. Glacier surge mechanisms inferred from ground-penetrating radar: Kongsvegen, Svalbard. *Journal of Glaciology*, 49(167):473–480, Dec. 2003. ISSN 00221430. doi: 10.3189/172756503781830458.

T. Yasuda and M. Furuya. Short-term glacier velocity changes at West Kunlun Shan, Northwest Tibet, detected by Synthetic Aperture Radar data. *Re-*

mote Sensing of Environment, 128:87–106, Jan. 2013. ISSN 00344257. doi: 10.1016/j.rse.2012.09.021.

J. C. Yde and N. T. Knudsen. 20th-century glacier fluctuations on Disko Island (Qeqertarsuaq), Greenland. *Annals of Glaciology*, 46(1):209–214, Oct. 2007. ISSN 02603055. doi: 10.3189/172756407782871558.

J. C. Yde and O. y. Paasche. Reconstructing Climate Change: Not All Glaciers Suitable. *Eos, Transactions American Geophysical Union*, 91(21):189, 2010. ISSN 0096-3941. doi: 10.1029/2010EO210001.

W. Zhang. Identification of glaciers with surge characteristics on the Tibetan Plateau. *Annals of Glaciology*, 16:168–172, 1992.

W. Zhang, R. An, H. Yang, and K. Jiao. Conditions of glacier development and some glacial features in the West Kunlun Mountains. *Bulletin of Glacier Research*, 7: 49–58, 1989.

Z. Zhang and K. Jiao. Modern glaciers on the south slope of West Kunlun Mountains (in Aksayqin Lake and Guozha Co Lake drainage areas). *Bulletin of glacier research*, 5:85–91, 1987.

B. Zheng. Preliminary studies of Quaternary glaciation and palaeogeography on the south slope of West Kunlun. *Bulletin of glacier research*, 5:93–102, 1987.

B. Zheng, H. Fushimi, K. Jiao, and S. Li. Characteristics of basal till and the discov-

ery of tephra layers in the West Kunlun Mountains. *Bulletin of glacier research*, 7:177–186, 1989.